Redox Biology 73 (2024) 103174

Contents lists available at ScienceDirect

Redox Biology

journal homepage: www.elsevier.com/locate/redox

The absence of the ribosomal protein Rpl2702 elicits the MAPK-mTOR signaling to modulate mitochondrial morphology and functions

Ling Liu [a,b], Yifan Wu [a,b], Ke Liu [a,b], Mengdan Zhu [a,b], Shouhong Guang [a,b], Fengsong Wang [c], Xing Liu [a,b], Xuebiao Yao [a,b], Jiajia He [a,b,**], Chuanhai Fu [a,b,*]

[a] MOE Key Laboratory for Cellular Dynamics & Center for Advanced Interdisciplinary Science and Biomedicine of IHM, Division of Life Sciences and Medicine, University of Science and Technology of China, Hefei, 230027, China
[b] Anhui Key Laboratory of Cellular Dynamics and Chemical Biology & Hefei National Research Center for Interdisciplinary Sciences at the Microscale, School of Life Sciences, University of Science and Technology of China, Hefei, 230027, China
[c] Department of Biology, School of Life Sciences, Anhui Medical University, Hefei, 230032, China

ARTICLE INFO

Keywords:
Mitochondria
MAPK
mTOR
Ribosome
Schizosaccharomyces pombe

ABSTRACT

Ribosomes mediate protein synthesis, which is one of the most energy-demanding activities within the cell, and mitochondria are one of the main sources generating energy. How mitochondrial morphology and functions are adjusted to cope with ribosomal defects, which can impair protein synthesis and affect cell viability, is poorly understood. Here, we used the fission yeast *Schizosaccharomyces Pombe* as a model organism to investigate the interplay between ribosome and mitochondria. We found that a ribosomal insult, caused by the absence of Rpl2702, activates a signaling pathway involving Sty1/MAPK and mTOR to modulate mitochondrial morphology and functions. Specifically, we demonstrated that Sty1/MAPK induces mitochondrial fragmentation in a mTOR-independent manner while both Sty1/MAPK and mTOR increases the levels of mitochondrial membrane potential and mitochondrial reactive oxygen species (mROS). Moreover, we demonstrated that Sty1/MAPK acts upstream of Tor1/TORC2 and Tor1/TORC2 and is required to activate Tor2/TORC1. The enhancements of mitochondrial membrane potential and mROS function to promote proliferation of cells bearing ribosomal defects. Hence, our study reveals a previously uncharacterized Sty1/MAPK-mTOR signaling axis that regulates mitochondrial morphology and functions in response to ribosomal insults and provides new insights into the molecular and physiological adaptations of cells to impaired protein synthesis.

1. Introduction

Ribosomes are organelles mediating protein translation, which is one of the most energy-demanding activities within the cell. Generally, eukaryotic ribosomes consist of two subunits, i.e., 40S and 60S subunits, which comprise ribosomal proteins and rRNA [1]. In addition to translation, ribosomal proteins play roles in many extraribosomal functions, such as cell proliferation, differentiation, apoptosis, and DNA damage repair [2]. Malfunctions of ribosomal proteins can cause hematological, metabolic, and cardiovascular diseases [2–5], as well as specific genetic disorders known as ribosomopathies [6]. Since mitochondria are the powerhouse of the cell [7], it is conceivable that ribosomal and mitochondrial functions are coordinated to maintain cellular fitness and viability. However, the molecular mechanisms and physiological consequences of the interplay between ribosomes and mitochondria are poorly understood.

Malfunctions of ribosomes can generate ribotoxic stress [8,9], which impairs protein synthesis and affect cell viability. To cope with ribotoxic stress, cells activate the signaling pathway involving the conserved mitogen-activated protein kinase (MAPK) [8,9]. Cells also activate the MAPK signaling pathway in response to various environmental stimuli. Upon activation, the MAPK signaling pathway promotes adaptive responses to restore cellular homeostasis [10]. In mammalian cells, three main MAPKs are present, namely ERK, JNK, and p38. Generally, ERK1/2 MAPKs are activated by growth factors to regulate cell growth and survival. JNK and p38 MAPKs, also known as stress-activated protein

* Corresponding author. MOE Key Laboratory for Cellular Dynamics & Center for Advanced Interdisciplinary Science and Biomedicine of IHM, Division of Life Sciences and Medicine, University of Science and Technology of China, Hefei, 230027 China.
** Corresponding author.
E-mail addresses: hejiajia@mail.ustc.edu.cn (J. He), chuanhai@ustc.edu.cn (C. Fu).

https://doi.org/10.1016/j.redox.2024.103174
Received 5 April 2024; Received in revised form 17 April 2024; Accepted 27 April 2024
Available online 29 April 2024

kinases (SAPK), are activated by various environmental stimuli, including UV and gamma radiation, oxidative stress, osmotic stress, and heat shock [11]. Similarly, in the model organism *Schizosaccharomyces Pombe*, three types of MAPK pathways were present. Among them, the Byr1-Spk1 pathway is required to promote mating and sporulation [12–14]. The Wis1-Spc1/Sty1 pathway is required to mediate stress responses, and is recognized as the counterpart of the p38 MAPK pathway in *Schizosaccharomyces Pombe* [15–19]. The Skh1-Spm1/Pmk1 pathway is required to regulate morphogenesis and integrity of the cell wall and is recognized as the counterpart of the ERK MAPK pathway in *Schizosaccharomyces Pombe* [16,20–22]. Whether and how MAPK signaling modulates mitochondrial functions in response to ribosomal defects or stress remains unclear.

Ribosomal functions are also relevant to the mammalian target of rapamycin (mTOR) signaling pathway. mTOR is an evolutionarily conserved kinase and functions to promote anabolism [23]. While mammals possess only one mTOR, *Schizosaccharomyces Pombe* possesses two mTOR proteins, i.e., Tor1 and Tor2 [24]. In mammals, mTOR forms two complexes: TORC1, which comprises mTOR, raptor, and mLST8 [25,26], and TORC2, which comprises mTOR, rictor, mSIN1, mLST8, and PRR5/PRR5L [27]. TORC1, but not TORC2, is inhibited by rapamycin. In *Schizosaccharomyces Pombe*, Tor2 forms TORC1 with Mip1 (Raptor in mammals), Wat1/Pop3 (Lst8 in mammals), Tco89, and Tor1 forms TORC2 with Ste20 (Rictor in mammals), Wat1/Pop3, Sin1, and Bit61 [28,29]. TORC1 is activated by amino acids and other stimuli. Upon activation, TORC1 promotes protein synthesis by phosphorylating ribosomal protein S6 kinases (S6Ks) and eukaryotic translation initiation factor 4E-binding proteins (4E-BP) [30]. TORC2 can be activated by ribosomes via direct interaction [31–33], and regulates various cellular functions such as cell polarity, cytoskeleton organization, and stress responses. However, the impact of ribosomal abnormalities on mTOR signaling remains unclear and warrants further investigation.

Given that the fission yeast *Schizosaccharomyces pombe* shares many conserved mitochondrial features with human cells [34,35], we used *Schizosaccharomyces pombe* as a model organism to dissect the interplay between ribosomes and mitochondria. We found that deletion of almost half of nonessential genes encoding ribosomal proteins, including Rpl2702, caused mitochondrial fragmentation. In the present study, we focused on Rpl2702 as a representative example of nonessential ribosomal proteins. We showed that the absence of Rpl2702 altered mitochondrial morphology in a MAPK-dependent manner and affected mitochondrial functions in a mTOR-dependent manner. We also revealed that the MAPK pathway is required to activate Tor1/TORC2 and Tor2/TORC1 in cells lacking Rpl2702. Thus, our study uncovered a novel mechanism by which ribosomes modulate mitochondrial morphology and functions via a MAPK-mTOR signaling axis in response to ribosomal stress.

2. Results

2.1. The absence of Rpl2702 causes mitochondrial fragmentation and alters mitochondrial function

The fission yeast *Schizosaccharomyces pombe* genome encodes approximately 58 and 85 proteins that form the small and large complexes of ribosomes, respectively. According to PomBase (http://www.pombase.org), 126 of these genes are nonessential. We microscopically examined mitochondrial morphology in 108 ribosomal gene-deleted strains derived from the single-gene deletion mutant library [36], and found that 50 mutants exhibited mitochondrial fragmentation as a predominant phenotype (Fig. S1). This means that the absence of ribosomal genes in almost half of the ribosomal gene-deleted strains affects mitochondrial morphology. This finding motivated us to further dissect the interplay between ribosomes and mitochondria. Among the ribosomal mutants causing mitochondrial fragmentation, the nonessential ribosomal gene *rpl2702* encodes Rpl2702, which is present on the periphery of ribosomes and is conserved between yeasts and humans, and the human homolog of Rpl2702, i.e., Rpl27, is highly relevant to diseases, including Diamond-Blackfan anemia and cancer [37,38]. Therefore, we chose Rpl2702 as a representative example of this study.

To confirm the mitochondrial phenotype resulting from the absence of Rpl2702, we compared wild-type (WT) and *rpl2702*-depleted (*rpl2702*Δ) cells, as well as *rpl2702*Δ cells ectopically expressing Rpl2702 from its own promoter at the *leu1* locus. We cultured the cells in Edinburgh Minimal Medium containing 2 % glucose and five supplements (adenine, histidine, leucine, lysine, and uracil) (referred to as EMM5S). To visualize mitochondria, Sdh2, a protein localizing within the mitochondrial matrix [39], was tagged with a green fluorescent protein (GFP). Microscopy revealed that mitochondria were tubular in WT cells but became fragmented in *rpl2702*Δ cells (Fig. 1A and B). Ectopic expression of Rpl2702 in *rpl2702*Δ cells restored tubular mitochondria (Fig. 1A and B). Dnm1 is the master regulator regulating mitochondrial fission [34]. To test whether mitochondrial fragmentation caused by the absence of Rpl2702 depends on Dnm1, we examined mitochondrial morphology in cells lacking both Rpl2702 and Dnm1, and mitochondria became tubular in the double-deletion cells (Fig. S2A). This result suggests that mitochondrial fragmentation caused by the absence of Rpl2702 depends on Dnm1. However, growth assays revealed that the growth of *rpl2702*Δ*dnm1*Δ and *rpl2702*Δ cells was almost comparable (Fig. S2B). These results indicate that mitochondrial fragmentation caused by the absence of Rpl2702 may not be the main factor affecting cell growth.

We then measured mitochondrial membrane potential and mitochondrial reactive oxygen species (referred to as mROS) by staining cells with DiOC6 and MitoSox, respectively. To ensure accuracy, we mixed WT and *rpl2702*Δ cells, each with Sid4 (a protein residing at the spindle pole body) tagged with tdTomato or GFP, and imaged the mixed cells on the same slide. As shown in Fig. 1C, the absence of Rpl2702 significantly increased mitochondrial membrane potential and slightly but significantly increased mROS levels (Fig. 1D). Ectopic expression of Rpl2702 in *rpl2702*Δ cells restored mitochondrial membrane potential (Fig. 1E) and mROS (Fig. 1F). In addition, we tested the effectiveness of three available mROS clearance chemicals, i.e., Trolox, mitoQ, and mitoTempo in detecting mROS, and found no noticeable difference (Figs. S2C–D). Therefore, in the present work, Trolox was used in assessing mROS. The increase in mROS in *rpl2702*Δ cells was not due to malfunctions of Sod2, a mitochondrial superoxide dismutase protein involved in the clearance of mROS because the protein level and localization of Sod2-GFP were comparable in WT and *rpl2702*Δ cells (Figs. S2E–F). Collectively, these results suggest that ribosome integrity is required to maintain mitochondrial morphology and functions.

2.2. The absence of Rpl2702 impairs ribosome assembly

In eukaryotes, ribosomes are assembled with small subunits (i.e., 40S) and large subunits (i.e., 60S) constituted with rRNA and proteins [1]. Therefore, it is reasonable to hypothesize that the absence of Rpl2702 impairs ribosome assembly.

To test the hypothesis, we first tested how the absence of Rpl2702 affected other ribosomal proteins, using the small subunit Rps2401 and the large subunit Rpl3002 as representative ribosomal components. As shown in Fig. 2A–D, the protein levels of both Rps2401 and Rpl3002 decreased significantly in *rpl2702*Δ cells. Similarly, within mitochondria, the protein levels of both Rps2401 and Rpl3002 decreased significantly in *rpl2702*Δ cells (Fig. 2E and F). We further assessed ribosome assembly by sucrose-gradient centrifugation (Fig. 2G). The result revealed that the amount of 60S- and 80S-ribosomal fractions decreased significantly in *rpl2702*Δ cells, suggesting that ribosome assembly is defective in *rpl2702*Δ cells. In addition, the amount of polysomes in *rpl2702*Δ cells decreased significantly, suggesting that active protein synthesis was attenuated in *rpl2702*Δ cells (Fig. 2G). Collectively, these results suggest that the absence of Rpl2702 impairs ribosomal assembly.

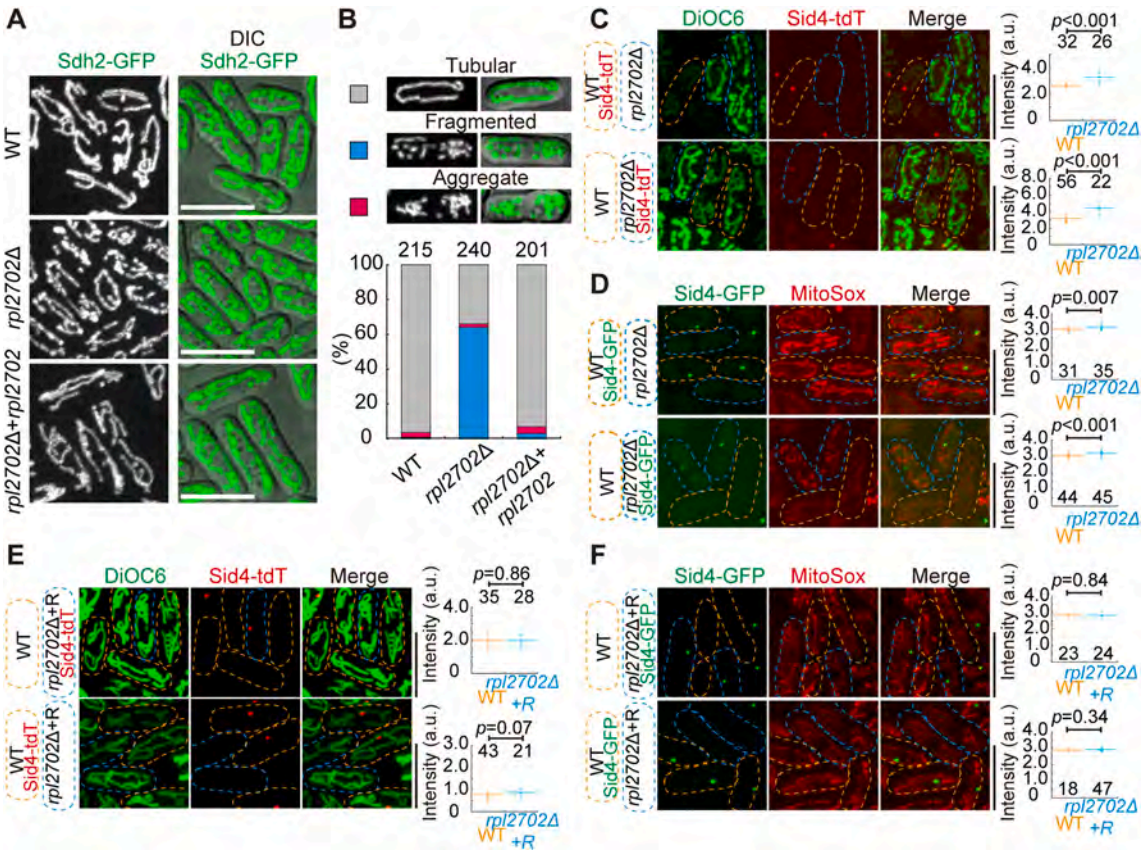

Fig. 1. The absence of Rpl2702 causes mitochondrial fragmentation and alters mitochondrial functions.

(A) Maximum projection images of wild-type (WT), *rpl2702*-depleted (*rpl2702*Δ), and *rpl2702Δ* cells ectopically expressing Rpl2702 from its own promoter at the *leu1* locus. The cells expressed GFP-tagged Sdh2 (Sdh2-GFP, a mitochondrial matrix protein) and were cultured in EMM5S medium. *DIC*, differential interference contrast. Scale bar, 10 μm

(B) Mitochondrial morphology quantification for the cells (A). Mitochondria were classified into three categories: tubular (grey), fragmented (blue), and aggregated (red). The percentage of each category is shown at the bottom of the graph, and the number of cells observed is indicated. Three independent experiments were performed, and the data shown are from a representative experiment.

(C) Maximum projection images of WT and *rpl2702Δ* cells stained with DiOC6 (3,3′-Dihexyloxacarbocyanine Iodide), a dye used to indicate mitochondrial membrane potential. Dashed lines mark cell contours. To compare DiOC6 signals accurately, WT cells expressing Sid4-tdTomato, a protein localizing to the spindle pole body (orange dashed lines), and *rpl2702*Δ cells (the absence of fluorescent labeling; blue dashed lines) were mixed and imaged (top panel). To exclude Sid4-tdTomato effects, WT cells (the absence of fluorescent labeling; orange dashed lines) and *rpl2702*Δ cells expressing Sid4-tdTomato (blue dashed lines) were mixed and imaged (bottom panel). The average intensity of DiOC6 staining was measured and quantified (right); the number of cells observed is indicated, and bars indicate the mean. The *p* values were calculated using the Wilcoxon-Mann-Whitney Rank Sum Test. Three independent experiments were performed, and shown is a representative experiment. Scale bar, 10 μm.

(D) Maximum projection images of WT and *rpl2702*Δ cells stained with MitoSox Red, a dye used to detect mitochondrial reactive oxygen species (mROS). Dashed lines mark cell contours. A similar approach of mixing cells, as demonstrated in (C), was employed to compare mROS signals. The average intensity of MitoSox staining was measured and quantified (right); the number of cells observed is indicated, and bars indicate the mean. The *p* values were calculated using the Wilcoxon-Mann-Whitney Rank Sum Test. Three independent experiments were performed, and shown is a representative experiment. Scale bar, 10 μm

(E) Maximum projection images of WT cells, and *rpl2702*Δ cells ectopically expressing Rpl2702 from its own promoter at the *leu1* locus. A similar approach of mixing cells, as demonstrated in (C), was employed. In the top panel, orange and blue dashed lines indicate WT cells (the absence of fluorescent labeling) and Sid4-tdTomato-expressing *rpl2702*Δ cells ectopically expressing Rpl2702, respectively. In the bottom panel, orange and blue dashed lines indicate Sid4-tdTomato-expressing WT cells, and *rpl2702*Δ cells ectopically expressing Rpl2702 (the absence of fluorescent labeling), respectively. The mixed cells were stained with DiOC6. Dashed lines mark cell contours. The average intensity of DiOC6 staining was measured and quantified on the right. The number of cells observed is indicated, and bars indicate the mean. The *p* values were calculated using the Wilcoxon-Mann-Whitney Rank Sum Test. Three independent experiments were performed, and shown is a representative experiment. Scale bar, 10 μm

(F) Maximum projection images of WT cells, and *rpl2702*Δ cells ectopically expressing Rpl2702 from its own promoter at the *leu1* locus. A similar approach of mixing cells, as demonstrated in (D), was employed. In the top panel, orange and blue dashed lines indicate WT cells (the absence of fluorescent labeling) and Sid4-GFP-expressing *rpl2702*Δ cells ectopically expressing Rpl2702, respectively. In the bottom panel, orange and blue dashed lines indicate Sid4-GFP-expressing WT cells, and *rpl2702*Δ cells ectopically expressing Rpl2702 (the absence of fluorescent labeling), respectively. The mixed cells were stained with MitoSox Red. Dashed lines mark cell contours. The average intensity of MitoSox Red staining was measured and quantified on the right. The number of cells observed is indicated, and bars indicate the mean. The *p* values were calculated using Student's *t*-test. Three independent experiments were performed, and shown is a representative experiment. Scale bar, 10 μm. (For interpretation of the references to colour in this figure legend, the reader is referred to the Web version of this article.)

2.3. The absence of Rpl2702 increases Sty1/MAPK activity

Mitochondria are the main source of cellular energy [7], and ribosomes require a large amount of energy to synthesize proteins [40]. Therefore, it is conceivable that mitochondria and the ribosome machine are intimately linked. To understand the link between mitochondria and the ribosome machine, we assessed four signaling pathways that are related to mitochondria and ribosome: MAPK, mTOR, PKA, and

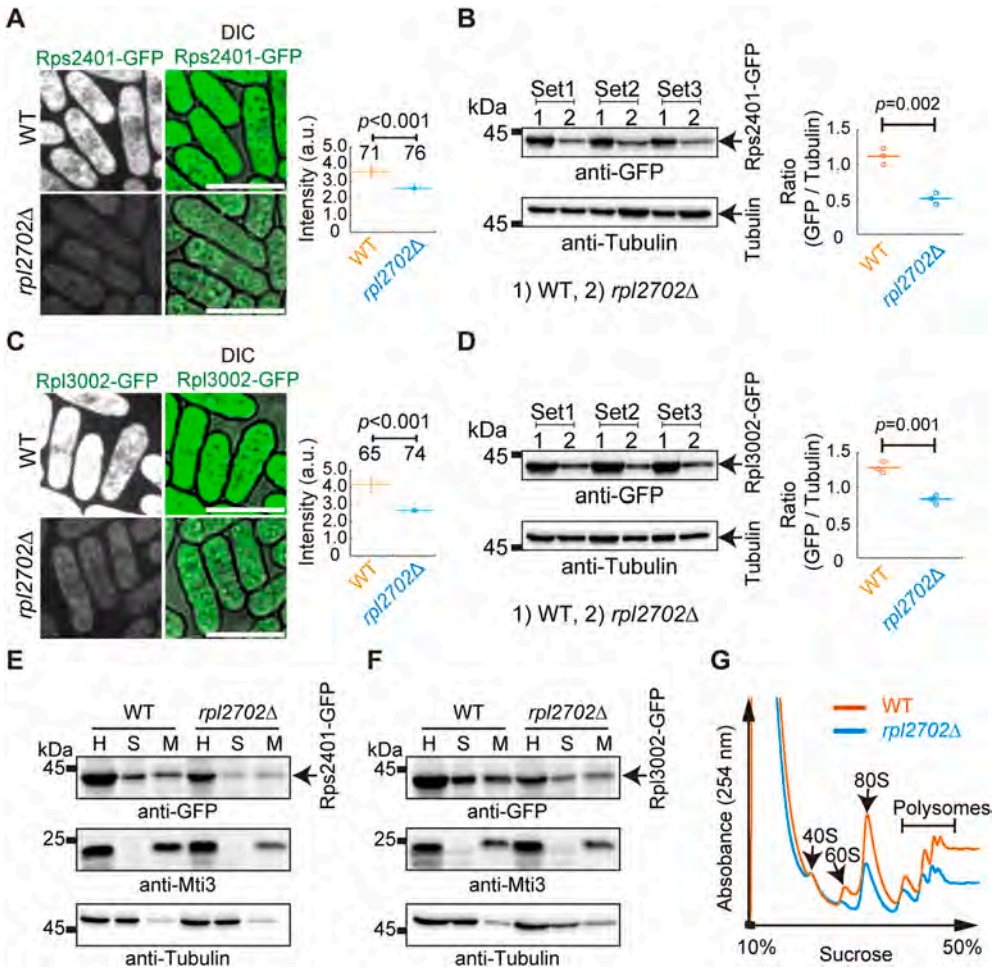

Fig. 2. The absence of Rpl2702 impairs ribosome assembly

(A) Maximum projection images of WT and *rpl2702*Δ cells expressing GFP-tagged Rps2401 (Rps2401-GFP, a ribosomal small subunit protein). The cells were cultured in EMM5S. The average intensity of Rps2401-GFP was measured and quantified (right). The number of cells observed is indicated, and bars indicate the mean. The *p* values were calculated using the Wilcoxon-Mann-Whitney Rank Sum Test. Three independent experiments were performed, and shown is a representative experiment. Scale bar, 10 μm

(B) Western blotting assays were performed to determine the protein levels of Rps2401-GFP in WT and *rpl2702*Δ cells. Antibodies against Rps2401-GFP and Tubulin were used. Data are from three sets of experiments, and the intensity ratio of Rps2401-GFP over Tubulin is quantified on the right. The *p* value was calculated using Student's *t*-test, and bars indicate the mean.

(C) Maximum projection images of WT and *rpl2702*Δ cells expressing GFP-tagged Rpl3002 (Rpl3002-GFP, a ribosomal large subunit protein). The cells were cultured in EMM5S medium. The average intensity of Rpl3002-GFP was measured and quantified (right). The number of cells observed is indicated, and bars indicate the mean. The *p* values were calculated using the Student's *t*-test. Three independent experiments were performed, and shown is a representative experiment. Scale bar, 10 μm.

(D) Western blotting assays were performed to determine the protein levels of Rpl3002-GFP in WT and *rpl2702*Δ cells. Antibodies against Rpl3002-GFP and Tubulin were used. Data are from three sets of experiments, and the intensity ratio of Rpl3002-GFP over Tubulin is quantified on the right. The *p* value was calculated using Student's *t*-test, and bars indicate the mean.

(E) Testing the protein levels of Rps2401-GFP within mitochondria in WT and *rpl2702*Δ cells. *H*, *S*, and *M* indicate whole-cell lysate, the cytosol fraction, and the mitochondria fraction, respectively. Mitochondria were isolated from WT and *rpl2702*Δ cells expressing Rps2401-GFP. Western blotting assays were performed with antibodies against GFP, Mti3, and Tubulin, respectively. A representative result from two independent experiments was shown here.

(F) Testing the protein levels of Rpl3002-GFP within mitochondria in WT and *rpl2702*Δ cells. *H*, *S*, and *M* indicate whole-cell lysate, the cytosol fraction, and the mitochondria fraction, respectively. Mitochondria were isolated from WT and *rpl2702*Δ cells expressing Rpl3002-GFP. Western blotting assays were performed with antibodies against GFP, Mti3, and Tubulin, respectively. A representative result from two independent experiments was shown here.

(G) Testing ribosome assembly by sucrose-gradient centrifugation. WT and *rpl2702*Δ cells were grown to exponential growth phase in EMM5S and were pretreated with 100 μg/mL cycloheximide for 15 min before harvesting. Whole cell extracts were resolved on 10–50 % sucrose gradients, and the absorbance at 254 nm was measured during fractionation. Positions of 40 S, 60 S, 80 S and polysomal species are indicated. Note that for comparison, the 40 S position of *rpl2702*Δ cells was normalized to that of WT cells.

AMPK (Fig. 3A and S3A). We found that the absence of Rpl2702 did not affect the signaling pathways of PKA and AMPK (Figs. S3B–C). By contrast, the absence of Rpl2702 significantly elevated the activity of MAPK and mTOR pathways (Fig. 3A and S3D). Therefore, we investigated how the activation of MAPK and mTOR influences mitochondrial morphology and function.

Among the three branches of MAPK signaling pathways, the p38 MAPK pathway responds to various environmental and intracellular stimuli and initiates adaptive responses [41]. In *Schizosaccharomyces pombe*, Sty1 is the counterpart of p38 MAPK, and its activation can be detected with an antibody against phosphorylated p38 [42]. Therefore, in the present work, we used this antibody to assess the activity of

Sty1/MAPK. We found that the absence of Rpl2702 significantly increased the phosphorylation (~1.5-fold increase, vs WT) and activation of Sty1/MAPK (Fig. 3A). This phenotype was not due to the alteration in the protein level of Sty1 because the protein level of Sty1-HA was comparable in WT and *rpl2702*Δ cells and *rpl2702*Δ cells ectopically expressing Rpl2702 from its own promoter (Fig. 3B). Interestingly, deletion of *sty1* in *rpl2702*Δ cells partially rescued the mitochondrial fragmentation phenotype (18.1 % of *rpl2702*Δ*sty1*Δ cells vs 61.4 % of *rpl2702*Δ cells) (Fig. 3C and D), suggesting that Sty1/MAPK is involved in mediating mitochondrial fragmentation. The protein level of Dnm1 was comparable in WT, *rpl2702*Δ, *sty1*Δ, and *rpl2702*Δ*sty1*Δ cells (Fig. S4A). However, the activity of Dnm1 appeared to be higher in *rpl2702*Δ cells than in WT, *sty1*Δ, and *rpl2702*Δ*sty1*Δ cells (Figs. S4B–C). These results further suggest that in *rpl2702*Δ cells, Sty1/MAPK regulates mitochondrial fragmentation by modulating Dnm1 activity. When we assessed mitochondrial membrane potential (Fig. 3E) and mROS (Fig. 3F), similar results were found. Specifically, deletion of *sty1* in *rpl2702*Δ cells (i.e., *rpl2702*Δ*sty1*Δ cells) significantly reduced the levels of both mitochondrial membrane potential (Fig. 3E) and mROS (Fig. 3F). Hence, we conclude that ribosomal impairments caused by the absence of Rpl2702 affect mitochondrial morphology and functions via Sty1/MAPK signaling (Fig. 3G).

2.4. The absence of Rpl2702 increases the activity of both Tor2/TORC1 and Tor1/TORC2

Unlike mammals, which use one mTOR kinase to assemble two mTOR complexes, i.e., TORC1 and TORC2 [23], *Schizosaccharomyces pombe* uses two mTOR kinases, namely Tor2 (the catalytic component of TORC1) and Tor1 (the catalytic component of TORC2). We measured Tor2/TORC1 activity by examining the phosphorylation of the Tor2/-TORC1 substrate S6K1 (Psk1 in *Schizosaccharomyces pombe*) with an antibody against phosphorylated S6K1 as previously reported [43,44]. We found that Tor2/TORC1 activity was higher in *rpl2702*Δ cells than WT cells, and that the increase in Tor2/TORC1 activity was abolished by rapamycin, an inhibitor of TORC1 (Fig. 4A–B and S5A-B). This phenotype was not due to the alteration in the protein level of Tor2 because the protein level of Flag-Tor2 was comparable in WT and *rpl2702*Δ cells and *rpl2702*Δ cells ectopically expressing Rpl2702 from its own promoter (Fig. 4C).

To assess Tor1/TORC2 activity, a kinase assay, as reported previously [45], was employed. Since the AGC kinase Gad8 is a substrate of Tor1/TORC2, Gad8 activity can be a proxy for assessment of Tor1/-TORC2 activity. Gad8 was immunoprecipitated and used in the *in vitro* kinase assays to assess its activity towards Fkh2, a substrate of Gad8. We found that Gad8 obtained from *rpl2702*Δ cells phosphorylated Fkh2-GST more than Gad8 obtained from WT cells (Fig. 4D and S5C), regardless of rapamycin treatment (Fig. 4E and S5D). This phenotype was not due to the alteration in the protein level of Tor1 because the protein level of Flag-Tor1 was comparable in WT and *rpl2702*Δ cells and *rpl2702*Δ cells ectopically expressing Rpl2702 from its own promoter (Fig. 4F). These results suggest that the absence of Rpl2702 increases Tor1/TORC2 activity independently of Tor2/TORC1.

To determine whether the Tor1/TORC2 activity is required to increase Tor2/TORC1 activity in *rpl2702*Δ cells, we measured the Tor2/TORC1 activity of WT, *rpl2702*Δ, *tor1*Δ, and *rpl2702*Δ*tor1*Δ cells by western blotting assays with the antibody against phosphorylated S6K1. We found that Tor2/TORC1 activity was increased in *rpl2702*Δ but did not change in *tor1*Δ and *rpl2702*Δ*tor1*Δ cells (Fig. 4G and S5E). Hence, the absence of Rpl2702 increased Tor2/TORC1 activity in a Tor1/TORC2-dependent manner but not vice versa (Fig. 4H).

2.5. The increased activity of Tor1/TORC2 in rpl2702Δ cells depends on Sty1/MAPK

Given that the absence of Rpl2702 activated both signaling pathways of Sty1/MAPK and Tor1/TORC2, we investigated the relationship between the two pathways by western blotting assays. We found that the activity of Sty1/MAPK in *rpl2702*Δ and *rpl2702*Δ*tor1*Δ cells was comparable (Fig. 5A), suggesting that Tor1/TORC2 was not required to activate Sty1/MAPK in *rpl2702*Δ cells. However, the activation of Tor1/TORC2 in *rpl2702*Δ cells depended on Sty1/MAPK because Gad8-HA purified from *rpl2702*Δ cells, but not *rpl2702*Δ*sty1*Δ cells, phosphorylated Fkh2-GST (Fig. 5B and S6). In addition, we tested whether the activation of Tor2/TORC1 in *rpl2702*Δ cells depended on Sty1/MAPK. As shown in Fig. 5C, the phosphorylation of the Tor2/TORC1 substrate Psk1 was detectable in *rpl2702*Δ, but not in *sty1*Δ and *rpl2702*Δ*sty1*Δ cells. Hence, the absence of Rpl2702 increased Tor2/TORC1 and Tor1/TORC2 activities in a Sty1/MAPK-dependent manner but not vice versa (Fig. 5D).

2.6. mTOR activation alters mitochondrial functions but not mitochondrial morphology in rpl2702Δ cells

mTOR functions downstream of Sty1/MAPK (Fig. 5), and Sty1/MAPK is required to regulate mitochondrial morphology and functions (Fig. 3). Therefore, we hypothesized that mTOR may directly regulate mitochondrial morphology and functions in cells lacking Rpl2702. To test this hypothesis, we observed mitochondrial morphology in cells lacking both Rpl2702 and Tor1/TORC2 (Fig. 6A and B) or in WT and *rpl2702*Δ cells treated with rapamycin (Fig. 6C and D). Quantification showed that neither the absence of Tor1/TORC2 nor inhibition of Tor2/TORC1 altered the mitochondrial fragmentation phenotype of *rpl2702*Δ cells (Fig. 6B and D). These results suggest that mTOR activity is not required to mediate mitochondrial fragmentation in *rpl2702*Δ cells.

Next, we measured mitochondrial respiration. Interestingly, the absence of Rpl2702 significantly decreased mitochondrial respiration in a Tor2/TORC1-dependent manner (Fig. 6E). This was consistent with the observation that the absence of Tsc2, a GTPase-activating protein functioning as an inhibitory factor of Tor2/TORC1 [46], similarly decreased mitochondrial respiration, which could be rescued by rapamycin treatment (Fig. 6E). Since the activity of Tor2/TORC1 in *rpl2702*Δ cells was increased in a Tor1/TORC2-dependent manner (Fig. 4H), we tested whether the decrease in mitochondrial respiration of *rpl2702*Δ cells also depends on Tor1/TORC2. As shown in Fig. 6F, the absence of Tor1/TORC2 in *rpl2702*Δ cells restored mitochondrial respiration to normal levels. Thus, we propose that Tor1/TORC2 and Tor2/TORC1 form a signaling pathway that modulates mitochondrial respiration.

Finally, we assessed the contribution of Tor1/TORC2 and Tor2/TORC1 to the regulation of mitochondrial membrane potential and mROS. As shown in Fig. 6G and H, the rapamycin-mediated inhibition of Tor2/TORC1 did not alter the increase in mitochondrial membrane potential and mROS in *rpl2702*Δ cells. By contrast, the absence of Tor1/TORC2 decreased mitochondrial membrane potential and mROS in *rpl2702*Δ cells (Fig. 6I and J). Collectively, Tor1/TORC2, but not Tor2/TORC1, is mainly responsible for the increased mitochondrial membrane potential and mROS in *rpl2702*Δ cells.

To test the specificity of the mitochondrial phenotypes caused by the absence of Rpl2702, we further examined mitochondrial phenotypes (i.e., mitochondrial morphology, membrane potential, and mROS) in cells lacking the small ribosomal subunit Rps602 or the large ribosomal subunit Rpl3601. Consistently, the absence of Rps602 or Rpl3601 caused mitochondrial fragmentation (Fig. S7A), increased mROS (Fig. S7C), and increased MAPK/Sty1 (Figs. S7D–E) and Tor2/mTORC1 (Figs. S7F–G) activities. The only difference is that the absence of Rpl3601 consistently increased mitochondrial membrane potential (Fig. S7B) whereas the absence of Rps602 decreased mitochondrial membrane potential (Fig. S7B). The different responses of mitochondrial membrane potential in cells lacking Rpl2702 (i.e., increase), Rpl3601 (i.e., increase), or Rps602 (i.e., decrease) indicate that mitochondrial membrane potential is a mitochondrial parameter affected by ribosomal

impairments in a context-dependent manner. The different responses of mitochondrial membrane potential also reflect the complexity and heterogeneity of ribosomes within the cell [47,48].

In conclusion, our data support the model that ribosomal impairments, caused by the absence of ribosomal nonessential subunits, lead to mitochondrial fragmentation and an increase in Sty1/MAPK and Tor2/mTORC1 activities and in mitochondrial ROS but lead to a heterogeneous effect on mitochondrial membrane potential.

2.7. The increased mitochondrial membrane potential and mROS are required to promote proliferation of *rpl2702Δ* cells

To understand the physiological significance of the increase in mitochondrial membrane potential and mROS in *rpl2702Δ* cells, we employed live-cell microscopy to directly examine cell proliferation (Fig. 7A). The absence of Rpl2702 caused slow cell growth (Fig. 7B and C). The antioxidant Trolox, which lowers ROS levels, had opposite effects on WT and *rpl2702Δ* cells. Specifically, Trolox treatment enhanced WT cell growth but inhibited *rpl2702Δ* cell growth (Fig. 7B). This

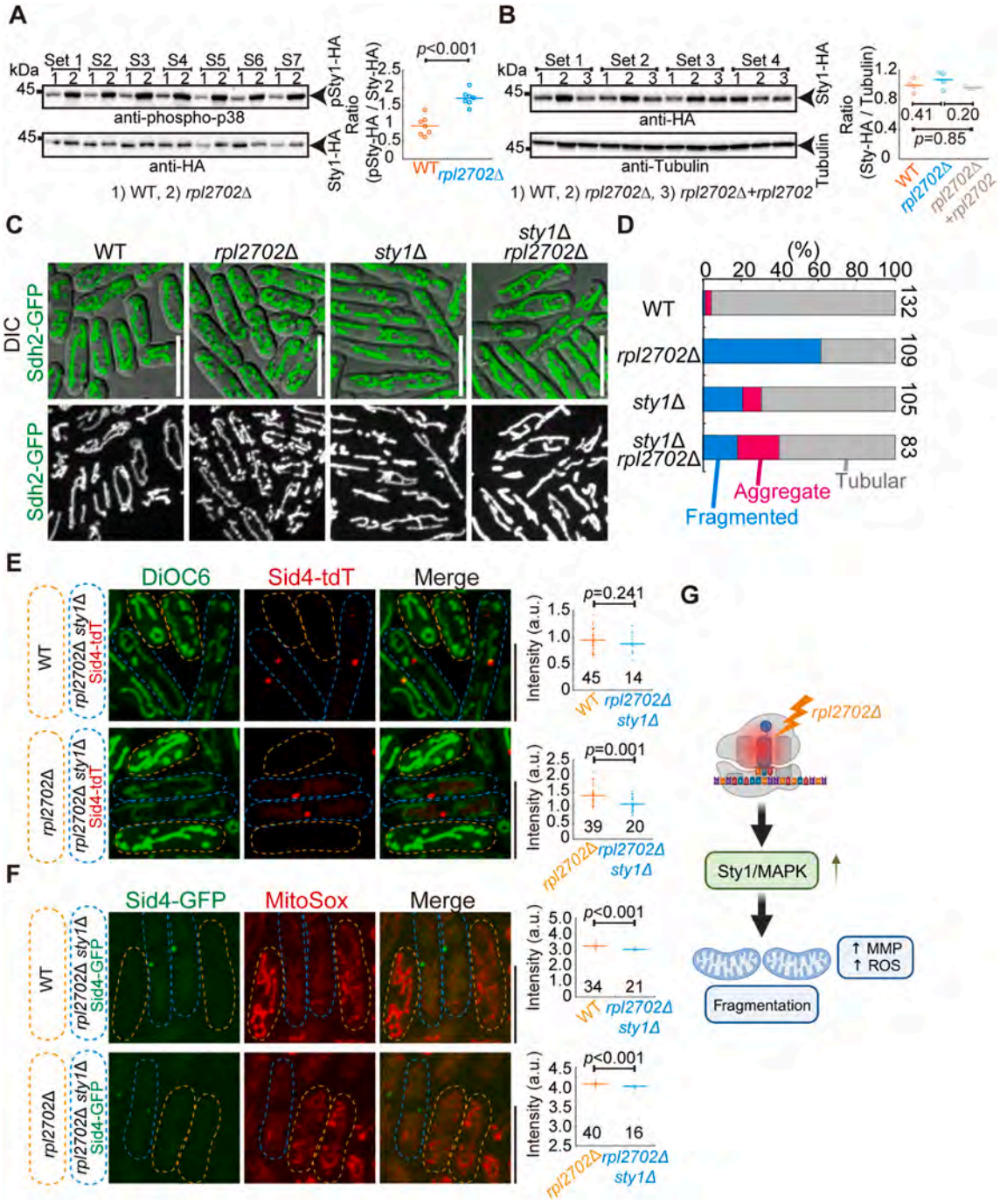

(caption on next page)

Fig. 3. The absence of Rpl2702 activates Sty1 and requires Sty1 activity for maintaining mitochondrial membrane potential and mROS levels.
(A) Western blotting assays were performed to measure Sty1 activity in WT and *rpl2702Δ* cells. Both types of cells expressed Sty1-HA. Antibodies against phospho-p38 (the phosphorylation form of Sty1) and HA were used. Data are from seven sets of experiments, and the intensity ratio of phospho-p38 over HA is quantified on the right. The *p* value was calculated using Student's *t*-test, and bars indicate the mean.
(B) Testing the protein levels of Sty1 in WT and *rpl2702Δ* cells and *rpl2702Δ* cells ectopically expressing Rpl2702 from its own promoter at the *leu1* locus. All cells expressed Sty1-HA. Antibodies against HA and Tubulin were used. Data are from four sets of experiments, and the intensity ratio of HA over Tubulin is quantified on the right. The *p* values were calculated using One-way ANOVA with the Tukey HSD Post Hoc test, and bars indicate the mean.
(C) Maximum projection images of WT, *rpl2702*Δ, *sty1*Δ and *rpl2702*Δ*sty1*Δ cells. The cells expressed Sdh2-GFP and were cultured in EMM5S. *DIC*, differential interference contrast. Scale bar, 10 μm.
(D) Mitochondrial morphology quantification for the cells in (C). The categories of mitochondrial morphology are indicated.
(E) Maximum projection images of the indicated cells stained with DiOC6. Cells were mixed as in Fig. 1C. Dashed lines mark cell contours. In the top panel, orange and blue dashed lines indicate WT cells (the absence of fluorescent labeling) and *rpl2702Δsty1Δ* Sid4-tdTomato-expressing cells, respectively. In the bottom panel, orange and blue dashed lines indicate *rpl2702Δ* cells (the absence of fluorescent labeling) and *rpl2702Δsty1Δ* Sid4-tdTomato-expressing cells, respectively. The average intensity of DiOC6 staining was measured and quantified (right); the number of cells observed is indicated, and bars indicate the mean. The *p* values were calculated using the Wilcoxon-Mann-Whitney Rank Sum Test. Three independent experiments were performed, and shown is a representative experiment. Scale bar, 10 μm
(F) Maximum projection images of the indicated cells stained with MitoSox Red. Cells were mixed as in Fig. 1D. Dashed lines mark cell contours. In the top panel, orange and blue dashed lines indicate WT cells (the absence of fluorescent labeling) and *rpl2702Δsty1Δ* Sid4-GFP-expressing cells, respectively. In the bottom panel, orange and blue dashed lines indicate *rpl2702Δ* cells (the absence of fluorescent labeling) and *rpl2702Δsty1Δ* Sid4-GFP-expressing cells, respectively. The average intensity of MitoSox Red staining was measured and quantified (right); the number of cells observed is indicated, and bars indicate the mean. The *p* values were calculated using the Wilcoxon-Mann-Whitney Rank Sum Test. Three independent experiments were performed, and shown is a representative experiment. Scale bar, 10 μm
(G) A diagram is shown to summarize the data in this figure: the absence of Rpl2702 causes mitochondrial fragmentation and increases mitochondrial membrane potential and mROS in a Sty1-dependent manner. (For interpretation of the references to colour in this figure legend, the reader is referred to the Web version of this article.)

finding suggests that higher mROS levels are required to promote *rpl2702*Δ cell proliferation.

The potent uncoupler FCCP, which uncouples mitochondrial oxidative phosphorylation and reduces mitochondrial membrane potential, similarly inhibited the growth of both WT and *rpl2702*Δ cells (Fig. 7C). This finding indicates that mitochondrial membrane potential plays an important role in promoting proliferation of both WT and *rpl2702*Δ cells. Given that *rpl2702*Δ*sty1*Δ or *rpl2702*Δ*tor1*Δ cells have a low level of mROS than *rpl2702*Δ cells (Fig. 3F and 6J), we further tested the long-term effect of the increase in mROS on cell growth (Fig. 7D). The results revealed that the growth of *rpl2702*Δ*sty1*Δ or *rpl2702*Δ*tor1*Δ was slightly slower than that of *rpl2702*Δ cells on EMM5S control plates (i.e., DMSO). Consistently, the growth of *rpl2702*Δ cells was slower than that of WT cells on EMM5S plates containing Trolox (clearance of mROS) (Fig. 7D). Interestingly, the growth of *rpl2702*Δ*sty1*Δ or *rpl2702*Δ*tor1*Δ was faster than that of *rpl2702*Δ cells, suggesting that the double deletion cells are less sensitive to Trolox treatment than *rpl2702*Δ cells. Collectively, the results support the conclusion that the increase in mROS plays a crucial role in promoting the growth of *rpl2702*Δ cells.

3. Discussion

The relationship between ribosomes and mitochondria is poorly understood. In the present work, we identify a Sty1/MAPK-mTOR signaling axis that regulates mitochondrial functions in response to ribosomal impairments in the fission yeast *Schizosaccharomyces pombe* (Fig. 7E).

In response to ribosomal impairments, *Schizosaccharomyces pombe* activates Sty1/MAPK signaling to module mitochondrial morphology and functions. Evidently, the absence of Rpl2702, a ribosomal component, activates Sty1/MAPK signaling (Fig. 3A), and causes mitochondrial fragmentation (Fig. 3C and D), increases mitochondrial membrane potential (Fig. 3E), and elevates mROS levels (Fig. 3F), all of which depend on Sty1/MAPK activity. In mammalian cells, three surveillance systems govern ribosomal functions and respond to ribosomal stress [8]: 1) the Ribosome-associated Quality Control (RQC), 2) the Integrated Stress Response (ISR), and 3) the Ribotoxic Stress Response (RSR). Among these systems, the RSR system involves the activation of p38 and JNK MAPK pathways and appears to be conserved in only mammalian cells [8]. In the RSR system, ribotoxic/ribosomal stress is sensed by the MAPKKK kinase ZAKα that physically interacts with ribosomes [8]. No ortholog of ZAKα is present in yeasts, including *Schizosaccharomyces pombe*, which may be the reason why the RSR system is not conserved in yeasts. Despite the absence of ZAKα in *Schizosaccharomyces pombe*, ribosomal impairments, caused by the absence of the ribosomal component Rpl2702, still activates the Sty1/MAPK signaling pathway (evident by the increased phosphorylation of Sty1 (Fig. 3A)), which is analogous to the p38 MAPK signaling pathway in mammals. Hence, yeasts may have alternative mechanisms to sense ribosomal stress and activate the MAPK signaling pathway. The molecular details of these mechanisms remain to be explored.

Ribosomal impairments activate mTOR signaling in a Sty1/MAPK-dependent manner in the fission yeast *Schizosaccharomyces pombe*. The interaction between MAPK and mTOR signaling pathways is complex, involving cross-inhibition and cross-activation [49]. For example, ERK/MAPK suppresses the mTOR signaling pathway to control bone formation in osteoblasts [50], while p38/MAPK-mediated mTOR activation protects ischemic cardiomyocytes [51]. In *Schizosaccharomyces pombe*, Sty1/MAPK was reported to positively regulate mTOR activity, but this regulation is not related to the direct interaction between Sty1/MAPK and mTOR [52]. Therefore, we speculate that Sty1/MAPK may regulate mTOR activity indirectly. In the present work, we demonstrate that ribosomal impairments trigger Sty1/MAPK-mediated activation of both Tor1/TORC2 and Tor2/TORC1 (Fig. 5). Moreover, we demonstrate that ribosomal impairments induce Tor2/TORC1 activation in a Tor1/TORC2-dependnent manner but not vice versa (Fig. 4). These findings reveal that a Sty1/MAPK-mTOR signaling axis operates in fission yeast cells to cope with ribosomal stress.

It is unlikely that the Sty1/MAPK-mTOR signaling is specifically induced by the absence of only Rpl2702 because the Sty1/MAPK-mTOR signaling is also induced by the absence of Rps602 (Figs. S7D and S7F) or Rpl3601 (Figs. S7E and S7G). Since that the absence of Rpl2702 decreases the protein levels of other ribosomal subunits such as Rps2401 and Rpl3002 (Fig. 2A–F) and impairs ribosome assembly (Fig. 2G). We speculate that defects in ribosome assembly may generally induce the activation of the Sty1/MAPK-mTOR signaling axis to cope with ribosomal stress.

The activated Sty1/MAPK-mTOR signaling axis affects mitochondria in different ways. In cells lacking Rpl2702, mitochondria became fragmented and show increased mitochondrial membrane potential and mROS levels (Fig. 1). Both Tor1/TORC2 and Sty1/MAPK are required to increase mitochondrial membrane potential and mROS levels (Fig. 3E, F,

and 6I-J). By contrast, Sty1/MAPK, but not Tor1/TORC2 and Tor2/TORC1, is involved in mitochondrial fragmentation (Fig. 3C, D, and 6A-D). The mechanisms of MAPK-mediated mitochondrial regulation are unclear, but mTOR, particularly TORC1, is known to promote mitochondrial biogenesis and respiration and regulate mitochondrial dynamics through transcriptional/translational control [53–55]. Interestingly, we found that Tor2/TORC1 and Tor1/TORC2 reduces mitochondrial respiration in response to ribosomal impairments (Fig. 6E and F). This may be an adaptive response to the expected decrease in protein synthesis in response to ribosomal impairments.

Why are mitochondrial membrane potential and mROS levels increased in response to ribosomal impairments? The increase in mitochondrial membrane potential may have beneficial effects on cytosolic proteostasis and mitochondrial-cytoplasmic communication, as mitochondrial membrane potential plays a crucial role in directing the import of cytosolic proteins into mitochondria for degradation or signaling [56]. ROS are crucial signaling molecules at physiological levels [57]. Thus, we speculate that ribosomal impairments trigger an increase in mROS, which in turn promote signaling within the cell to cope with ribosomal stress. Consistently, we found that reducing mROS levels or mitochondrial membrane potential worsened the growth of cells bearing defective ribosomes (Fig. 7B–D). Future studies should elucidate the mechanisms by which mitochondrial membrane potential and mROS modulate the adaptive response to ribosomal impairments.

4. Conclusions

In the present study, we revealed an uncharacterized signaling axis, involving Sty1/MAPK and mTOR, that regulates mitochondrial functions in response to ribosomal impairments. Given that ribosomal abnormalities cause ribosomopathies, a group of human disorders, the present work may provide insights into developing MAPK or mTORC-

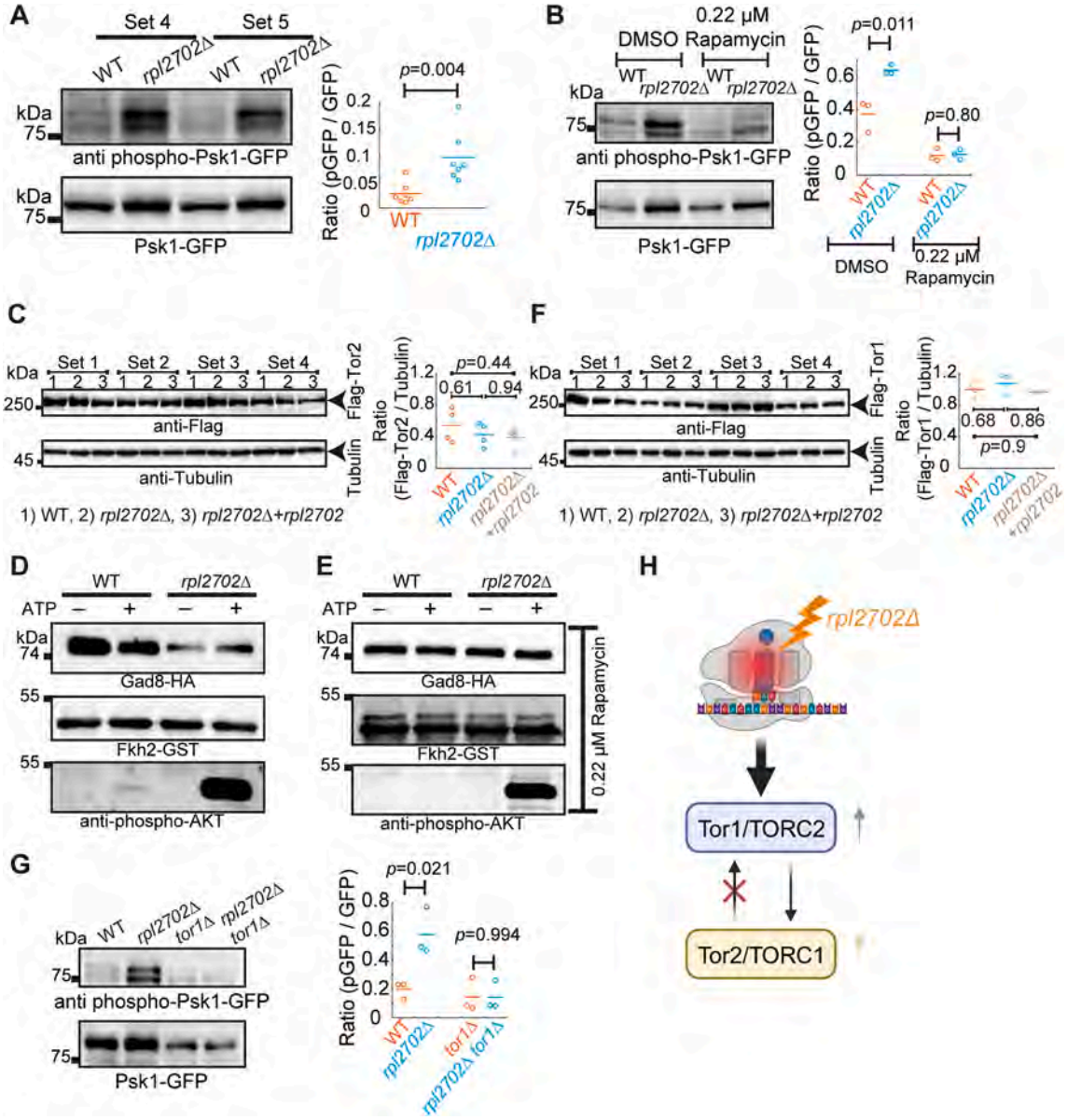

(caption on next page)

Fig. 4. The absence of Rpl2702 activates mTOR.

(A) Western blotting assays were performed to measure mTORC1 (Tor2 in fission yeasts) activity with antibodies against phospho-p70 S6K (phospho-Psk1-GFP in the graph) and GFP. Note that Psk1, the substrate of Tor2, was tagged with GFP in WT and *rpl2702Δ* cells. Seven sets of independent experiments were performed (Fig. S5A), and two were shown here. The intensity ratio of phospho-p70 S6K over GFP is quantified on the right. The *p* value was calculated using Student's *t*-test, and bars indicate the mean.

(B) Western blotting analysis of mTORC1 activity in Psk1-GFP-expressing WT and *rpl2702Δ* cells treated with or without 0.22 μM rapamycin (mTORC1 inhibitor for 1 h). Antibodies against phospho-p70 S6K (phospho-Psk1-GFP in the graph) and GFP were used. A representative result from three independent experiments (Fig. S5B) was shown here. The intensity ratio of phospho-p70 S6K over GFP is quantified on the right. The *p* value was calculated using Student's *t*-test, and bars indicate the mean. Note that the absence of Rpl2702 increased mTORC1 activity and rapamycin treatment inhibited mTORC1 activity in WT and *rpl2702Δ* cells.

(C) Testing the protein levels of Tor2 in WT and *rpl2702Δ* cells and *rpl2702Δ* cells ectopically expressing Rpl2702 from its own promoter at the *leu1* locus. All cells expressed Flag-Tor2. Antibodies against Flag and Tubulin were used. Data are from four sets of experiments, and the intensity ratio of Flag over Tubulin is quantified on the right. The *p* values were calculated using One-way Anova with the Tukey HSD Post Hoc test, and bars indicate the mean.

(D) Western blotting analysis of mTORC2 activity in WT and *rpl2702Δ* cells. The mTORC2 substrate, kinase Gad8, was purified from the indicated cells by immunoprecipitation and used for *in vitro* kinase assays with the Gad8 substrate of Gad8, i.e., Fkh2(291–426)-GST, purified from *E.coli*. A phospho-specific antibody against phospho-Fkh2 at Ser-456 (i.e., anti-phospho-AKT) was used to detect Fkh2 phosphorylation by Gad8. A representative result from three independent experiments (Fig. S5C) was shown here. Note that the absence of Rpl2702 increased mTORC2 activity in the reaction containing ATP.

(E) Western blotting analysis of mTORC2 activity in WT and *rpl2702Δ* cells treated with or without 0.22 μM rapamycin. Note that the presence of Rapamycin, i.e., the inhibition of mTORC1, had no notable effect on the increased activity of mTORC2 by the absence of Rpl2702. A representative result from three independent experiments (Fig. S5D) was shown here.

(F) Testing the protein levels of Tor1 in WT and *rpl2702Δ* cells and *rpl2702Δ* cells ectopically expressing Rpl2702 from its own promoter at the *leu1* locus. All cells expressed Flag-Tor1. Antibodies against Flag and Tubulin were used. Data are from four sets of experiments, and the intensity ratio of Flag over Tubulin is quantified on the right. The *p* values were calculated using One-way Anova with the Tukey HSD Post Hoc test, and bars indicate the mean.

(G) Western blotting analysis of mTORC1 activity in Psk1-GFP-expressing WT, *rpl2702*Δ, *tor1*Δ and *rpl2702*Δ*tor1*Δcells. Antibodies against phospho-p70 S6K (phospho-Psk1-GFP in the graph) and GFP were used. Note that no mTORC1 activity was detected in cells lacking *tor1* (mTORC2). A representative result from three independent experiments (Fig. S5E) were shown here. The intensity ratio of phospho-p70 S6K over GFP is quantified on the right. The *p* value was calculated using Student's *t*-test, and bars indicate the mean

(H) Diagram showing the interplay between Tor1 (i.e., mTORC2). and Tor2 (i.e., mTORC1) in cells lacking Rpl2702. The absence of Rpl2702 activates Tor1 and Tor2, and Tor2 activation depends on Tor1 but not vice versa.

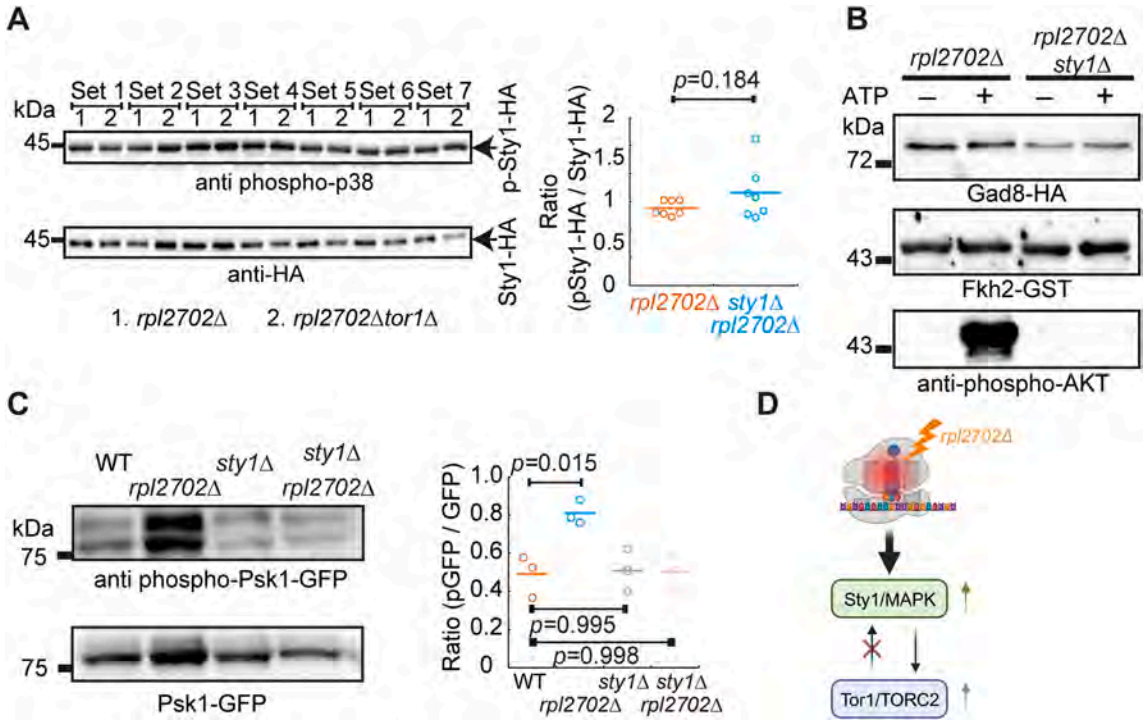

Fig. 5. The activation of Tor1 in cells lacking Rpl2702 depends on Sty1 but not vice versa.

(A) Western blotting analysis of Sty1 activity in *rpl2702*Δ and *rpl2702*Δ*tor1*Δ cells expressing Sty1-HA. Antibodies against phospho-p38 and HA were used. Seven sets of experiments were performed. The intensity ratio of phospho-p38 over HA in (A) was quantified on the right. The *p* value was calculated using Student's *t*-test, and bars indicate the mean.

(B) *In vitro* kinase assays of Tor1 activity in *rpl2702Δ* and *rpl2702*Δ*sty1*Δ cells. A representative result from four independent experiments (Fig. S6) was shown here. Note that the absence of Rpl2702, but not the absence of both Rpl2702 and Sty1, increased mTORC2 activity in the reaction containing ATP.

(C) Western blotting analysis of mTORC1/Tor2 activity in Psk1-GFP-expressing WT, *rpl2702*Δ, *sty1*Δ and *rpl2702*Δ*sty1*Δcells. Antibodies against phospho-p70 S6K (phospho-Psk1-GFP in the graph) and GFP were used. Note that no mTORC1 activity was detected in cells lacking *sty1* (MAPK). A representative result from three independent experiments were shown here. The intensity ratio of phospho-p70 S6K over GFP is quantified on the right. The *p* value was calculated using One-way Anova with the Tukey HSD Post Hoc test, and bars indicate the mean

(D) Diagram showing the interplay between Tor1 (i.e., mTORC2). and Sty1 (i.e., MAPK) in cells lacking Rpl2702. The absence of Rpl2702 activates Tor1, and Sty1, and Tor1 activation depends on Sty1 but not vice versa.

based strategies for intervening the relevant conditions.

5. Materials and methods

5.1. Yeast strains and plasmids

Yeast strains were created by random spore digestion or tetra-dissection methods. Genes were deleted or tagged with the pFA6a series of plasmids by PCR-based homologous recombination. Strains were cultured in Edinburgh Minimal Media (EMM) containing 2 % glucose and five supplements: adenine, leucine, uracil, histidine and lysine (0.225 g/L each) (referred to as EMM5S). Supplementary Table S1 lists the yeast strains and plasmids used in this study. All culture media were purchased from Formedium (www.formedium.com).

5.2. Live-cell microscopy and data analysis

All imaging data were acquired at room temperature by Volocity on a

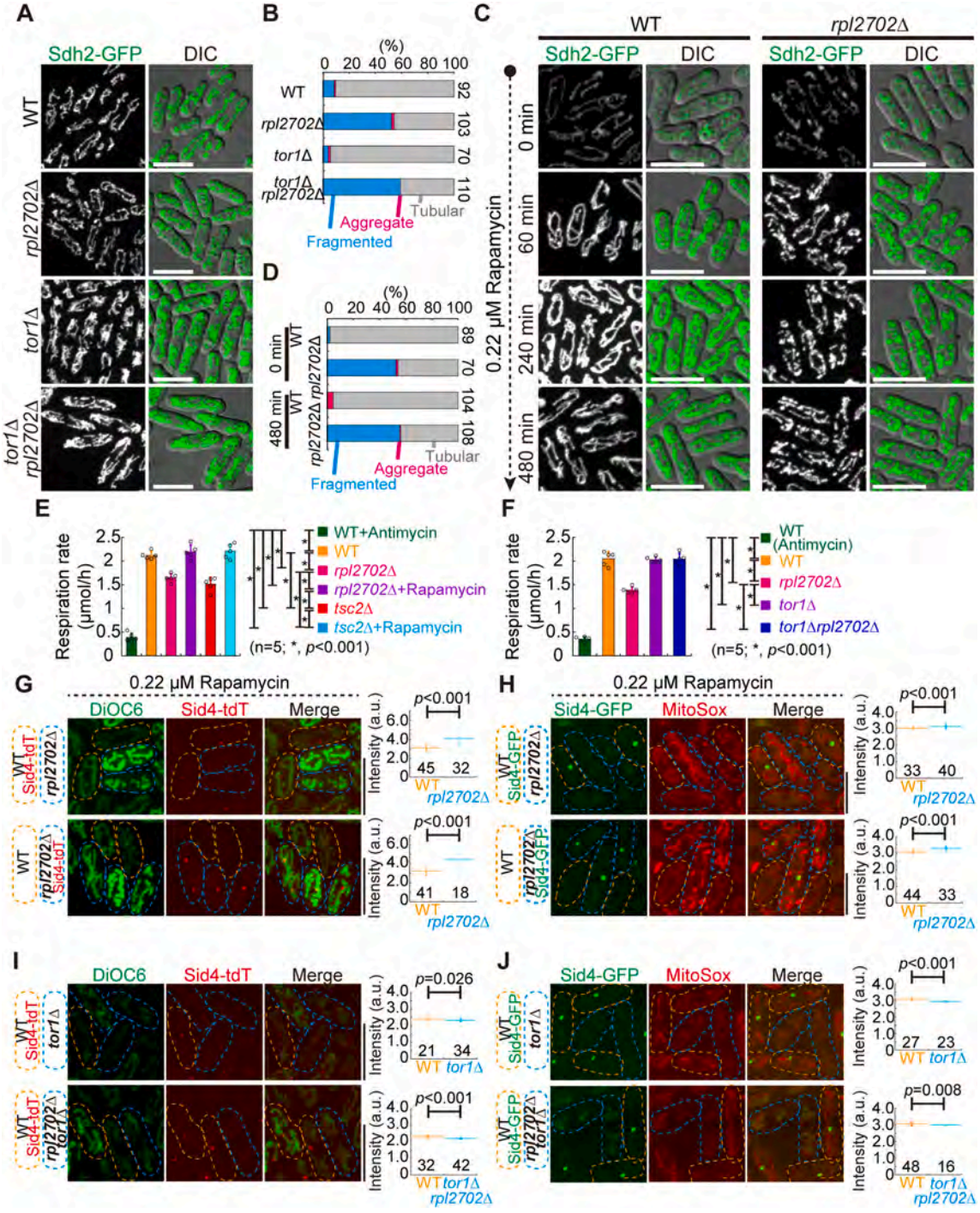

(caption on next page)

Fig. 6. High mTOR activity in *rpl2702*Δ affects mitochondrial respiration and mitochondrial membrane potential and mROS, but not mitochondrial morphology.
(A) Maximum projection images of WT, *rpl2702*Δ, *tor1*Δ, and *rpl2702*Δ*tor1*Δ cells. The cells were cultured in EMM5S medium, and mitochondria were visualized by expressing Sdh2-GFP. *DIC*, differential interference contrast. Scale bar, 10 μm
(B) Quantification of mitochondrial morphology for the cells in (A), and the number of cells analyzed is indicated.
(C) Maximum projection images of WT and *rpl2702*Δ cells expressing Sdh2-GFP. The cells were treated with 0.22 μM Rapamycin. Cells were collected and imaged at 0, 1, 4, and 8 h after the treatment. *DIC*, differential interference contrast. Scale bar, 10 μm.
(D) Quantification of mitochondrial morphology for the cells in (C), and the number of cells analyzed is indicated.
(E) The respiration rate of the indicated cells. A Strathkelvin oxygen respirometer was used to measure the respiration rate, and five independent experiments were performed. The *p* values were calculated by One-way ANOVA with Post Hoc Tukey HSD test. Antimycin A (a potent inhibitor of the electron transport chain) was used as a negative control while *tsc2Δ* cells (with constitutive Tor2 activation) were used as a positive control. Note that rapamycin treatment increased the respiration rates of *rpl2702*Δ and *tsc2*Δ cells.
(F) The respiration rate of the indicated cells. Five independent experiments were performed, and the *p* values were calculated by One-way ANOVA with Post Hoc Tukey HSD test. Antimycin A was used as a negative control. Note that the absence of Tor1 increased the respiration rate of *rpl2702Δ* cells.
(G) Maximum projection images of WT and *rpl2702Δ* cells treated with 0.22 μM Rapamycin. To visualize mitochondrial membrane potential, the cells were stained with DiOC6. A similar approach of mixing cells, as in Fig. 1C, was used here. Dashed lines mark cell contours. In the top panel, orange and blue dashed lines indicate WT Sid4-tdTomato-expressing cells and *rpl2702*Δ cells (without fluorescent labeling), respectively. In the bottom panel, orange and blue dashed lines indicate WT cells (without fluorescent labeling) and *rpl2702*Δ Sid4-tdTomato-expressing cells, respectively. The average intensity of DiOC6 staining was measured and quantified (shown on the right); the number of cells observed is indicated, and bars indicate the mean. The *p* values were calculated using the Wilcoxon-Mann-Whitney Rank Sum Test. Three independent experiments were performed, and shown is a representative experiment. Scale bar, 10 μm
(H) Maximum projection images of WT and *rpl2702Δ* cells treated with 0.22 μM Rapamycin. To visualize mitochondrial ROS, the cells were stained with MitoSox Red. A similar approach of mixing cells, as in Fig. 1D, was used here. Dashed lines mark cell contours. In the top panel, orange and blue dashed lines indicate WT Sid4-GFP-expressing cells and *rpl2702*Δ cells (without fluorescent labeling), respectively. In the bottom panel, orange and blue dashed lines indicate WT cells (without fluorescent labeling) and *rpl2702*Δ Sid4-GFP-expressing cells, respectively. The average intensity of MitoSox Red staining was measured and quantified (shown on the right); the number of cells observed is indicated, and bars indicate the mean. The *p* values were calculated using the Wilcoxon-Mann-Whitney Rank Sum Test. Three independent experiments were performed, and shown is a representative experiment. Scale bar, 10 μm.
(I) Maximum projection images of the indicated cells. To visualize mitochondrial membrane potential, the cells were stained with DiOC6. A similar approach of mixing cells, as in Fig. 1C, was used here. Dashed lines mark cell contours. In the top panel, orange and blue dashed lines indicate WT Sid4-tdTomato-expressing cells and *tor1*Δ cells (without fluorescent labeling), respectively. In the bottom panel, orange and blue dashed lines indicate WT Sid4-tdTomato-expressing cells and *rpl2702*Δ*tor1*Δ cells (without fluorescent labeling), respectively. The average intensity of DiOC6 staining was measured and quantified (shown on the right); the number of cells observed is indicated, and bars indicate the mean. The *p* values were calculated using the Wilcoxon-Mann-Whitney Rank Sum Test. Three independent experiments were performed, and shown is a representative experiment. Scale bar, 10 μm
(J) Maximum projection images of the indicated cells. To visualize mitochondrial ROS, the cells were stained with MitoSox. A similar approach of mixing cells, as in Fig. 1D, was used here. Dashed lines mark cell contours. In the top panel, orange and blue dashed lines indicate WT Sid4-GFP-expressing cells *tor1*Δ cells (without fluorescent labeling), respectively. In the bottom panel, orange and blue dashed lines indicate WT Sid4-GFP-expressing cells and *rpl2702*Δ*tor1*Δ cells (without fluorescent labeling), respectively. The average intensity of MitoSox staining was measured and quantified (shown on the right); the number of cells observed is indicated, and bars indicate the mean. The *p* values were calculated using the Wilcoxon-Mann-Whitney Rank Sum Test. Three independent experiments were performed, and shown is a representative experiment. Scale bar, 10 μm. (For interpretation of the references to colour in this figure legend, the reader is referred to the Web version of this article.)

PerkinElmer ultraview spinning-disk confocal microscope equipped with a Nikon Apochromat TIRF 100X 1.49NA objective and a Hamamatsu C9100–23B EMCCD camera (www.perkinelmer.com). For maximum projection images, stack images containing 11 planes at 0.5 μm spacing were taken. Data were analyzed with MetaMorph 7.7 (www.moleculardevices.com) and ImageJ 1.52 (NIH, Bethesda, MD, USA). Graphs were generated and statistical analysis was performed with KaleidaGraph 4.5 (www.synergy.com). Diagram illustrations were created with BioRender.com.

5.3. Assessment of cell growth

To determine the doubling time of cells, live-cell microscopy was performed to observe cell growth and division on an EMM5S agar pad, and images were acquired every 5 min. The doubling time was calculated as the interval between two consecutive septations.

To assess cell growth on plates, cells were first cultured overnight in EMM5S medium at 30 °C. When the optical density (OD) of cells at 600 nm (referred to as OD_{600}) reached 0.6–0.8, the cells were then collected, diluted (10-fold series of dilution), and spotted on EMM5S plates containing Trolox or DMSO. The plates were incubated at 30 °C for 3 days, and images were taken using the Tanon 1600 Gel Image System (www.biotanon.com).

5.4. Oxygen consumption assays

Oxygen consumption of cells was measured with a Strathkelvin respirometer (Model 782) (Strathkelvin, Lanarkshire), following the manufacturer instructions. A 1.5 mL EMM5S culture at room temperature was used for each measurement. Antimycin A (ALX-380-075-M005, Enzo Life Sciences), an inhibitor of the electron transport chain, was added at a working concentration of 0.15 μg/mL as a control.

5.5. Measurement of mitochondrial membrane potential

To measure the mitochondrial membrane potential, cells were stained with DiOC6 (3,3′-Dihexyloxacarbocyanine Iodide) (D273, ThermoFisher) at a working concentration of 0.175 mM. Cells were grown in EMM5S until they reached the exponential phase (OD_{600} 0.6–0.8), and stained with DiOC6 for 15 min at 30 °C in the dark. After centrifugation and washing with fresh EMM5S, the stained cells were analyzed by microscopy.

5.6. Measurement of mitochondrial reactive oxygen species

To measure the mitochondrial reactive oxygen species, cells were stained with MitoSox Red (M36008, ThermoFisher), a mitochondrial superoxide indicator dye, at a working concentration of 5 μM. Cells were grown in EMM5S until they reached the exponential phase (OD_{600} 0.6–0.8), and stained with MitoSox for 30 min at 30 °C in the dark. After centrifugation and washing with fresh EMM5S, the stained cells were analyzed by microscopy.

5.7. β-galactosidase activity assays

Strains bearing the fbp1-LacZ plasmid were cultured overnight in

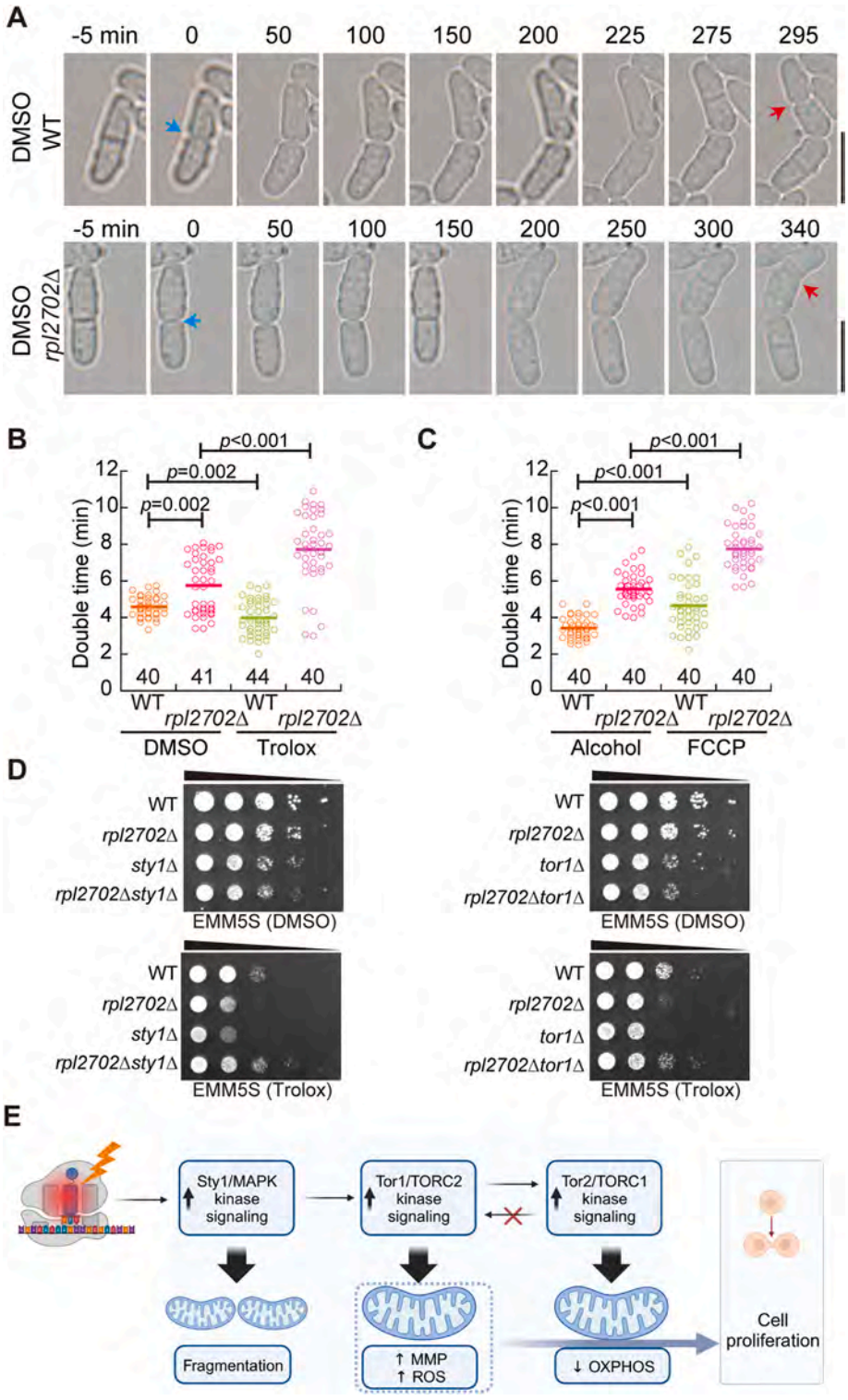

(caption on next page)

Fig. 7. The increased mitochondrial membrane potential and mROS production are required for *rpl2702*Δ cell growth.
(A) Representative bright-field time-lapse images of WT and *rpl2702*Δ cells treated with DMSO. Images were acquired every 5 min. Blue and red arrows indicate parental and daughter cells undergoing septation, respectively. Note that the doubling time of *rpl2702*Δ cells is longer than that of WT cells. Scale bar, 5 μm
(B) Quantification of the doubling time of the indicated cells. WT and *rpl2702*Δ cells were treated with 1 mM Trolox or its solvent DMSO. The number of cells analyzed is indicated, and bars indicate the mean. The *p* values were calculated using the Wilcoxon-Mann-Whitney Rank Sum Test. Two independent experiments were performed, and shown is a representative experiment.
(C) Quantification of the doubling time of the indicated cells. WT and *rpl2702*Δ cells were treated with 5 μM FCCP or its solvent alcohol. The number of cells analzyed is indicated, and bars indicate the mean. The *p* values were calculated using the Wilcoxon-Mann-Whitney Rank Sum Test. Two independent experiments were performed, and shown is a representative experiment.
(D) Growth assays for WT, *rpl2702*Δ, *sty1*Δ, *rpl2702*Δ*sty1*Δ, *tor1*Δ, and *rpl2702*Δ*tor1*Δ cells. The indicated cells were spotted on EMM5S plates containing 1 mM Trolox and its solvent DMSO after 10-fold serial dilution.
(E) A model illustrating the role of Rpl2702 in regulating mitochondrial functions. The absence of Rpl2702 causes ribosomal impairments, which promotes mitochondrial fragmentation in a Sty1/MAPK-dependent manner. As a result, Sty1/MAPK activates Tor1/mTORC2 to increases mitochondrial membrane potential and mROS, which in turn activates Tor2/mTORC1 to reduce mitochondrial respiration. The increased mitochondrial membrane potential and mROS are required for regulating cell proliferation. (For interpretation of the references to colour in this figure legend, the reader is referred to the Web version of this article.)

EMM5S medium at 30 °C until they reached the exponential phase (OD_{600} 0.6–0.8). Cells were collected for measuring galactosidase activity using a yeast-galactosidase assay kit (75768, ThermoFisher) in a 96-well plate, as described previously [58].

5.8. Protein extraction and immunoblotting

To analyze protein expression, cells were incubated in EMM5S overnight until OD_{600} reached 0.6–0.8. Approximate 10 mL cells were collected and washed once with ddwater. Subsequently, protein extract from the washed cells was prepared by the TCA lysis method. Specifically, cells were resuspended in 50 μl 20 % TCA and lysed with 200 μl 0.5 mm glass beads (BioSpec) using a mixer mill (Retsch MM400) (www.retsch.com). Another 50 μl 20 % TCA was added to the cell lysate, which was then mixed with 400 μl 5% TCA and centrifuged at 12,000 rpm for 10 min at 4 °C. The supernatant was collected and mixed with 175 μl SDS sample buffer (62.5 mM Tris-Cl, pH = 6.8, 2 % SDS, 10 % glycerol, 0.1 % Bromphenol blue, and 300 mM 2-Mercaptoethanol) and 25 μl 1.5 M Tris (pH = 8.8). The mixture was boiled at 100 °C for 5 min. Samples were separated by SDS-PAGE and then immunoblotted with antibodies against Tubulin (dilution factor, 1:10,000; 63–160, Bio Academia), GFP (dilution factor, 1:2000; 600-101-215, Rockland), FLAG (dilution factor, 1:1000; M20008S, Abmart), Phospho-AMPKα (Thr172) (dilution factor, 1:1000; 2535, Cell Signaling Technology), Phospho-p38 MAPK (Thr180/Tyr182) (dilution factor, 1:1000; 4511, Cell Signaling Technology), phospho-p70 S6 Kinase (Thr389) (dilution factor, 1:1000; 9206, Cell Signaling Technology), and Dnm1(dilution factor, 1:1000; Homemade).

5.9. In vitro kinase assays

To assess Tor1/TORC2 activity, *in vitro* kinase assays were performed as described previously [45,59]. Specifically, a GST-fused peptide of Fkh2 (residues 291–411) was expressed in an *Escherichia coli* BL21 using pGEX-6p-1 vector and purified. Yeast cells expressing Gad8-HA were grown in EMM5S overnight until OD_{600} reached 0.6–0.8 and harvested approximate 1 L of cells. The cells were washed once with ddwater and ground in liquid nitrogen with a mortar grinder (RM 200, www.retsch.com). After grinding, the cells were lysed in Tris-buffered saline (TBS) buffer containing 0.2 % Triton X-100, cocktail protease inhibitors, and 1 mM phenylmethylsulfonyl fluoride at 4 °C for 30 min with gentle rotation. The cell lysates were then centrifuged at 12,000 rpm at 4 °C for 30 min, and the supernatants were collected. Dynabeads protein G beads (1004D, ThermoFisher) bound with an antibody against HA (11867423001, Roche) were added to the supernatants and the mixture was incubated at 4 °C on a rotator for 2 h. The Dynabeads protein G beads were then washed with TBST buffer (Tris-buffered saline buffer plus 0.1 % Triton X-100) five times and TBS once. The Dynabeads protein G beads were resuspended in 30 μl of kinase buffer (50 mM Tris-HCl, 10 mM $MgCl_2$, 1 mM EGTA, 2 mM dithiothreitol, 200 μM ATP and 0.01 % Brij 35; pH 7.5) with 0.1 μg of GST-Fkh2 at 30 °C for 1 h. The reaction was stopped by adding SDS sample buffer and boiling at 100 °C for 5 min, followed by analysis by western blotting with antibodies against HA (dilution factor, 1:1000; 11867423001, Roche), GST (dilution factor, 1:10,000; AE006, Abclonal), and phospho-AKT substrate (dilution factor, 1:1000; 9611, Cell Signaling Technology).

5.10. Mitochondria isolation

To isolate mitochondria, cells were incubated in EMM5S overnight until OD_{600} reached 0.6–0.8. Cells (20 mL) were collected and washed twice with ddwater, and mitochondria were isolated with the Mitochondria Yeast Isolation Kit (ab178779, Abcam). fractionation samples of whole cell lysate, the cytoplasmic fraction, and the mitochondrial fraction were boiled at 100 °C for 5 min. The samples were separated by SDS-PAGE and then analyzed by immunoblotting with antibodies against GFP (dilution factor, 1:2000; 600-101-215, Rockland), Mti3 (dilution factor, 1:2000; Homemade) and Tubulin (dilution factor, 1:10,000; 63–160, Bio Academia).

5.11. Ribosome assembly and polysome analyses by sucrose-gradient centrifugation

Cells were incubated in EMM5S overnight until OD_{600} reached 0.6–0.8, 100 μg/mL cycloheximide (94271, Amresco) was added to the medium for 15 min at 30 °C, and 100 mL cells were collected and washed three times with Diethyl pyrocarbonate (DEPC)-treated water (B600154-0025, Sangon). Subsequently, the cells were resuspended in ice-cold 600 μL lysis buffer (20 mM Tris-HCl (pH 7.5), 150 mM NaCl, 5 mM MgCl2, 1 % Triton X-100, 200 μg/mL cycloheximide, 20 units/mL RNase inhibitors, cocktail protease inhibitors (EDTA-free), and 1 mM dithiothreitol), and lysed with 200 μL ice-cold 0.5 mm glass beads (BioSpec) using a mixer mill (Retsch MM400) (www.retsch.com). The cell lysates were diluted with 400 μL lysis buffer, followed by two-step centrifugation: 1) at 4 °C, 16,000×*g*, 5 min, and 2) at 4 °C, 16,000×*g*, 15 min. Finally, 290 μL of the supernatants were layered onto sucrose gradient (10% – 50 %) solution dissolved in 15 mM Tris-HCl (pH 7.5), 15 mM $MgCl_2$, 300 mM NaCl, and 1 mM dithiothreitol, followed by centrifugation at 38,000 rpm for 2 h 45 min at 4 °C with the Beskman SW41 Ti rotor. The sample was fractionated by using an ISCO fractionator (Teledyne ISCO) for continuous record of the absorbance at 254 nm.

Funding

This work is supported by grants from National Key Research and Development Program of China [2022YFA1303100], National Natural Science Foundation of China [92354304, 32070707, and 31621002], the Fundamental Research Funds for the Central Universities [WK9110000151], and the Center for Advanced Interdisciplinary

Science and Biomedicine of IHM [QYPY20220003].

CRediT authorship contribution statement

Ling Liu: Writing – review & editing, Writing – original draft, Methodology, Investigation, Formal analysis. **Yifan Wu:** Investigation. **Ke Liu:** Investigation. **Mengdan Zhu:** Investigation. **Shouhong Guang:** Writing – review & editing, Methodology. **Fengsong Wang:** Writing – review & editing, Methodology. **Xing Liu:** Writing – review & editing, Methodology. **Xuebiao Yao:** Writing – review & editing, Methodology, Funding acquisition. **Jiajia He:** Writing – review & editing, Supervision, Investigation, Formal analysis. **Chuanhai Fu:** Writing – review & editing, Writing – original draft, Supervision, Methodology, Funding acquisition, Conceptualization.

Declaration of competing interest

The authors declare that they have no conflict of interest.

Data availability

Data will be made available on request.

Acknowledgments

We thank members in the Fu laboratory for insightful discussion and NBRP, Japan, for providing strains.

Appendix A. Supplementary data

Supplementary data to this article can be found online at https://doi.org/10.1016/j.redox.2024.103174.

References

[1] D.N. Wilson, J.H. Doudna Cate, The structure and function of the eukaryotic ribosome, Cold Spring Harb Perspect Biol 4 (2012).
[2] J.R. Warner, K.B. McIntosh, How common are extraribosomal functions of ribosomal proteins? Mol Cell 34 (2009) 3–11.
[3] A. Amsterdam, R.M. Nissen, Z. Sun, E.C. Swindell, S. Farrington, N. Hopkins, Identification of 315 genes essential for early zebrafish development, Proc Natl Acad Sci U S A. 101 (2004) 12792–12797.
[4] M.E. Casad, D. Abraham, I.M. Kim, S. Frangakis, B. Dong, N. Lin, M.J. Wolf, H. A. Rockman, Cardiomyopathy is associated with ribosomal protein gene haploinsufficiency in Drosophila melanogaster, Genetics 189 (2011) 861–870.
[5] W. Wang, S. Nag, X. Zhang, M.H. Wang, H. Wang, J. Zhou, R. Zhang, Ribosomal proteins and human diseases: pathogenesis, molecular mechanisms, and therapeutic implications, Med. Res. Rev. 35 (2015) 225–285.
[6] A. Narla, B.L. Ebert, Ribosomopathies: human disorders of ribosome dysfunction, Blood 115 (2010) 3196–3205.
[7] B. Westermann, Mitochondrial fusion and fission in cell life and death, Nat. Rev. Mol. Cell Biol. 11 (2010) 872–884.
[8] A.C. Vind, A.V. Genzor, S. Bekker-Jensen, Ribosomal stress-surveillance: three pathways is a magic number, Nucleic Acids Res. 48 (2020) 10648–10661.
[9] A.C. Vind, G. Snieckute, M. Blasius, C. Tiedje, N. Krogh, D.B. Bekker-Jensen, K. L. Andersen, C. Nordgaard, M.A.X. Tollenaere, A.H. Lund, J.V. Olsen, H. Nielsen, S. Bekker-Jensen, ZAKalpha recognizes stalled ribosomes through partially redundant sensor domains, Mol Cell 78 (2020) 700–713 e707.
[10] M. Gacto, T. Soto, J. Vicente-Soler, T.G. Villa, J. Cansado, Learning from yeasts: intracellular sensing of stress conditions, Int. Microbiol. 6 (2003) 211–219.
[11] M. Krishna, H. Narang, The complexity of mitogen-activated protein kinases (MAPKs) made simple, Cell. Mol. Life Sci. 65 (2008) 3525–3544.
[12] Y. Gotoh, E. Nishida, M. Shimanuki, T. Toda, Y. Imai, M. Yamamoto, Schizosaccharomyces pombe Spk1 is a tyrosine-phosphorylated protein functionally related to Xenopus mitogen-activated protein kinase, Mol. Cell Biol. 13 (1993) 6427–6434.
[13] D.A. Hughes, A. Ashworth, C.J. Marshall, Complementation of byr1 in fission yeast by mammalian MAP kinase kinase requires coexpression of Raf kinase, Nature 364 (1993) 349–352.
[14] T. Masuda, K. Kariya, M. Shinkai, T. Okada, T. Kataoka, Protein kinase Byr2 is a target of Ras1 in the fission yeast Schizosaccharomyces pombe, J. Biol. Chem. 270 (1995) 1979–1982.
[15] G. Degols, K. Shiozaki, P. Russell, Activation and regulation of the Spc1 stress-activated protein kinase in Schizosaccharomyces pombe, Mol. Cell Biol. 16 (1996) 2870–2877.
[16] P. Perez, J. Cansado, Cell integrity signaling and response to stress in fission yeast, Curr. Protein Pept. Sci. 11 (2010) 680–692.
[17] I. Samejima, S. Mackie, P.A. Fantes, Multiple modes of activation of the stress-responsive MAP kinase pathway in fission yeast, EMBO J. 16 (1997) 6162–6170.
[18] I. Samejima, S. Mackie, E. Warbrick, R. Weisman, P.A. Fantes, The fission yeast mitotic regulator win1+ encodes an MAP kinase kinase kinase that phosphorylates and activates Wis1 MAP kinase kinase in response to high osmolarity, Mol. Biol. Cell 9 (1998) 2325–2335.
[19] C. Widmann, S. Gibson, M.B. Jarpe, G.L. Johnson, Mitogen-activated protein kinase: conservation of a three-kinase module from yeast to human, Physiol. Rev. 79 (1999) 143–180.
[20] R. Loewith, A. Hubberstey, D. Young, Skh1, the MEK component of the mkh1 signaling pathway in Schizosaccharomyces pombe, J. Cell Sci. 113 (Pt 1) (2000) 153–160.
[21] A.S. Sengar, N.A. Markley, N.J. Marini, D. Young, Mkh1, a MEK kinase required for cell wall integrity and proper response to osmotic and temperature stress in Schizosaccharomyces pombe, Mol. Cell Biol. 17 (1997) 3508–3519.
[22] T. Zaitsevskaya-Carter, J.A. Cooper, Spm1, a stress-activated MAP kinase that regulates morphogenesis in S.pombe, EMBO J. 16 (1997) 1318–1331.
[23] S. Wullschleger, R. Loewith, M.N. Hall, TOR signaling in growth and metabolism, Cell 124 (2006) 471–484.
[24] J.L. Crespo, M.N. Hall, Elucidating TOR signaling and rapamycin action: lessons from Saccharomyces cerevisiae, Microbiol. Mol. Biol. Rev. 66 (2002) 579–591, table of contents.
[25] D.H. Kim, D.D. Sarbassov, S.M. Ali, J.E. King, R.R. Latek, H. Erdjument-Bromage, P. Tempst, D.M. Sabatini, mTOR interacts with raptor to form a nutrient-sensitive complex that signals to the cell growth machinery, Cell 110 (2002) 163–175.
[26] R. Loewith, E. Jacinto, S. Wullschleger, A. Lorberg, J.L. Crespo, D. Bonenfant, W. Oppliger, P. Jenoe, M.N. Hall, Two TOR complexes, only one of which is rapamycin sensitive, have distinct roles in cell growth control, Mol Cell 10 (2002) 457–468.
[27] N. Cybulski, M.N. Hall, TOR complex 2: a signaling pathway of its own, Trends Biochem. Sci. 34 (2009) 620–627.
[28] T. Hayashi, M. Hatanaka, K. Nagao, Y. Nakaseko, J. Kanoh, A. Kokubu, M. Ebe, M. Yanagida, Rapamycin sensitivity of the Schizosaccharomyces pombe tor2 mutant and organization of two highly phosphorylated TOR complexes by specific and common subunits, Gene Cell. 12 (2007) 1357–1370.
[29] T. Matsuo, Y. Otsubo, J. Urano, F. Tamanoi, M. Yamamoto, Loss of the TOR kinase Tor2 mimics nitrogen starvation and activates the sexual development pathway in fission yeast, Mol. Cell Biol. 27 (2007) 3154–3164.
[30] K. Hara, K. Yonezawa, Q.P. Weng, M.T. Kozlowski, C. Belham, J. Avruch, Amino acid sufficiency and mTOR regulate p70 S6 kinase and eIF-4E BP1 through a common effector mechanism, J. Biol. Chem. 273 (1998) 14484–14494.
[31] W.J. Oh, C.C. Wu, S.J. Kim, V. Facchinetti, L.A. Julien, M. Finlan, P.P. Roux, B. Su, E. Jacinto, mTORC2 can associate with ribosomes to promote cotranslational phosphorylation and stability of nascent Akt polypeptide, EMBO J. 29 (2010) 3939–3951.
[32] X. Xie, K.L. Guan, The ribosome and TORC2: collaborators for cell growth, Cell 144 (2011) 640–642.
[33] V. Zinzalla, D. Stracka, W. Oppliger, M.N. Hall, Activation of mTORC2 by association with the ribosome, Cell 144 (2011) 757–768.
[34] F. Dong, M. Zhu, F. Zheng, C. Fu, Mitochondrial fusion and fission are required for proper mitochondrial function and cell proliferation in fission yeast, FEBS J. 289 (2022) 262–278.
[35] F. Zheng, F. Dong, S. Yu, T. Li, Y. Jian, L. Nie, C. Fu, Klp2 and Ase1 synergize to maintain meiotic spindle stability during metaphase I, J. Biol. Chem. 295 (2020) 13287–13298.
[36] D.U. Kim, J. Hayles, D. Kim, V. Wood, H.O. Park, M. Won, H.S. Yoo, T. Duhig, M. Nam, G. Palmer, S. Han, L. Jeffery, S.T. Baek, H. Lee, Y.S. Shim, M. Lee, L. Kim, K.S. Heo, E.J. Noh, A.R. Lee, Y.J. Jang, K.S. Chung, S.J. Choi, J.Y. Park, Y. Park, H. M. Kim, S.K. Park, H.J. Park, E.J. Kang, H.B. Kim, H.S. Kang, H.M. Park, K. Kim, K. Song, K. Bin Song, P. Nurse, K.L. Hoe, Analysis of a genome-wide set of gene deletions in the fission yeast Schizosaccharomyces pombe, Nat. Biotechnol. 28 (2010) 617. U111.
[37] Y. Furuta, R.J. Tinker, A. Gulsevin, S.M. Neumann, R. Hamid, J.D. Cogan, L. Rives, Q. Liu, H.C. Chen, K.M. Joos, J.A. Phillips 3rd, N. Undiagnosed Diseases, Probable digenic inheritance of Diamond-Blackfan anemia, Am. J. Med. Genet. 194 (2024) e63454.
[38] S.Y. Park, D. Seo, E.H. Jeon, J.Y. Park, B.C. Jang, J.I. Kim, S.S. Im, J.H. Lee, S. Kim, C.H. Cho, Y.H. Lee, RPL27 contributes to colorectal cancer proliferation and stemness via PLK1 signaling, Int. J. Oncol. 63 (2023).
[39] D. Zhao, X.M. Liu, Z.Q. Yu, L.L. Sun, X. Xiong, M.Q. Dong, L.L. Du, Atg20- and Atg24-family proteins promote organelle autophagy in fission yeast, J. Cell Sci. 129 (2016) 4289–4304.
[40] M. Kafri, E. Metzl-Raz, G. Jona, N. Barkai, The cost of protein production, Cell Rep. 14 (2016) 22–31.
[41] B. Canovas, A.R. Nebreda, Diversity and versatility of p38 kinase signalling in health and disease, Nat. Rev. Mol. Cell Biol. 22 (2021) 346–366.
[42] F. Gaits, G. Degols, K. Shiozaki, P. Russell, Phosphorylation and association with the transcription factor Atf1 regulate localization of Spc1/Sty1 stress-activated kinase in fission yeast, Genes Dev. 12 (1998) 1464–1473.
[43] C. Corral-Ramos, R. Barrios, J. Ayte, E. Hidalgo, TOR and MAP kinase pathways synergistically regulate autophagy in response to nutrient depletion in fission yeast, Autophagy 18 (2022) 375–390.
[44] A. Nakashima, Y. Otsubo, A. Yamashita, T. Sato, M. Yamamoto, F. Tamanoi, Psk1, an AGC kinase family member in fission yeast, is directly phosphorylated and

controlled by TORC1 and functions as S6 kinase, J. Cell Sci. 125 (2012) 5840–5849.
[45] A. Cohen, M. Kupiec, R. Weisman, Glucose activates TORC2-Gad8 protein via positive regulation of the cAMP/cAMP-dependent protein kinase A (PKA) pathway and negative regulation of the Pmk1 protein-mitogen-activated protein kinase pathway, J. Biol. Chem. 289 (2014) 21727–21737.
[46] X. Gao, Y. Zhang, P. Arrazola, O. Hino, T. Kobayashi, R.S. Yeung, B. Ru, D. Pan, Tsc tumour suppressor proteins antagonize amino-acid-TOR signalling, Nat. Cell Biol. 4 (2002) 699–704.
[47] D. Li, J. Wang, Ribosome heterogeneity in stem cells and development, J. Cell Biol. 219 (2020).
[48] W. Li, J. Zhang, W. Cheng, Y. Li, J. Feng, J. Qin, X. He, Differential paralog-specific expression of multiple small subunit proteins cause variations in rpl42/eL42 incorporation in ribosome in fission yeast, Cells 11 (2022).
[49] M.C. Mendoza, E.E. Er, J. Blenis, The Ras-ERK and PI3K-mTOR pathways: cross-talk and compensation, Trends Biochem. Sci. 36 (2011) 320–328.
[50] J.M. Kim, Y.S. Yang, J. Hong, S. Chaugule, H. Chun, M.C.H. van der Meulen, R. Xu, M.B. Greenblatt, J.H. Shim, Biphasic regulation of osteoblast development via the ERK MAPK-mTOR pathway, Elife 11 (2022).
[51] G. Hernandez, H. Lal, M. Fidalgo, A. Guerrero, J. Zalvide, T. Force, C.M. Pombo, A novel cardioprotective p38-MAPK/mTOR pathway, Exp. Cell Res. 317 (2011) 2938–2949.
[52] S. Morigasaki, L.C. Chin, T. Hatano, M. Emori, M. Iwamoto, H. Tatebe, K. Shiozaki, Modulation of TOR complex 2 signaling by the stress-activated MAPK pathway in fission yeast, J. Cell Sci. 132 (2019).
[53] J.T. Cunningham, J.T. Rodgers, D.H. Arlow, F. Vazquez, V.K. Mootha, P. Puigserver, mTOR controls mitochondrial oxidative function through a YY1-PGC-1alpha transcriptional complex, Nature 450 (2007) 736–740.
[54] M. Morita, S.P. Gravel, V. Chenard, K. Sikstrom, L. Zheng, T. Alain, V. Gandin, D. Avizonis, M. Arguello, C. Zakaria, S. McLaughlan, Y. Nouet, A. Pause, M. Pollak, E. Gottlieb, O. Larsson, J. St-Pierre, I. Topisirovic, N. Sonenberg, mTORC1 controls mitochondrial activity and biogenesis through 4E-BP-dependent translational regulation, Cell Metab. 18 (2013) 698–711.
[55] M. Morita, J. Prudent, K. Basu, V. Goyon, S. Katsumura, L. Hulea, D. Pearl, N. Siddiqui, S. Strack, S. McGuirk, J. St-Pierre, O. Larsson, I. Topisirovic, H. Vali, H. M. McBride, J.J. Bergeron, N. Sonenberg, mTOR controls mitochondrial dynamics and cell survival via MTFP1, Mol Cell 67 (2017) 922–935 e925.
[56] L. Ruan, C. Zhou, E. Jin, A. Kucharavy, Y. Zhang, Z. Wen, L. Florens, R. Li, Cytosolic proteostasis through importing of misfolded proteins into mitochondria, Nature 543 (2017) 443–446.
[57] H. Sies, D.P. Jones, Reactive oxygen species (ROS) as pleiotropic physiological signalling agents, Nat. Rev. Mol. Cell Biol. 21 (2020) 363–383.
[58] F. Zheng, B. Jia, F. Dong, L. Liu, F. Rasul, J. He, C. Fu, Glucose starvation induces mitochondrial fragmentation depending on the dynamin GTPase Dnm1/Drp1 in fission yeast, J. Biol. Chem. 294 (2019) 17725–17734.
[59] C. Fu, J.J. Ward, I. Loiodice, G. Velve-Casquillas, F.J. Nedelec, P.T. Tran, Phospho-regulated interaction between kinesin-6 Klp9p and microtubule bundler Ase1p promotes spindle elongation, Dev. Cell 17 (2009) 257–267.